# Modal analysis of an operational offshore wind turbine using enhanced Kalman filter-based subspace identification

van Vondelen, Aemilius A.W.; Iliopoulos, Alexandros; Navalkar, Sachin T.; van der Hoek, Daan C.; van Wingerden, Jan Willem

**DOI**
10.1002/we.2849

**Publication date**
2023

**Document Version**
Final published version

**Published in**
Wind Energy

**Citation (APA)**
van Vondelen, A. A. W., Iliopoulos, A., Navalkar, S. T., van der Hoek, D. C., & van Wingerden, J. W. (2023). Modal analysis of an operational offshore wind turbine using enhanced Kalman filter-based subspace identification. *Wind Energy*, *26*(9), 923-945. https://doi.org/10.1002/we.2849

Received: 7 September 2022 | Revised: 12 April 2023 | Accepted: 11 June 2023

DOI: 10.1002/we.2849

RESEARCH ARTICLE

WILEY

# Modal analysis of an operational offshore wind turbine using enhanced Kalman filter-based subspace identification

Aemilius A. W. van Vondelen[1] | Alexandros Iliopoulos[2] | Sachin T. Navalkar[2] | Daan C. van der Hoek[1] | Jan-Willem van Wingerden[1]

[1]Delft Center for Systems and Control, Delft University of Technology, Delft, The Netherlands

[2]Siemens Gamesa Renewable Energy, The Hague, The Netherlands

**Correspondence**
Aemilius A. W. van Vondelen, Delft Center for Systems and Control, Delft University of Technology, Delft 2628 CD, The Netherlands.
Email: A.A.W.vanVondelen@tudelft.nl

**Funding information**
Not funded.

## Abstract

Operational modal analysis (OMA) is an essential tool for understanding the structural dynamics of offshore wind turbines (OWTs). However, the classical OMA algorithms require the excitation of the structure to be stationary white noise, which is often not the case for operational OWTs due to the presence of periodic excitation caused by rotor rotation. To address this issue, several solutions have been proposed in the literature, including the Kalman filter-based stochastic subspace identification (KF-SSI) method which eliminates harmonics through estimation and orthogonal projection. In this paper, an enhanced version of the KF-SSI method is presented that involves a concatenation step, allowing multiple datasets with similar environmental conditions to be used in the identification process, resulting in higher precision. This enhanced framework is applied to an operational OWT and compared to other OMA methods, such as the modified least-squares complex exponential and PolyMAX. Using field data from a multi-megawatt operational OWT, it is shown that the enhanced framework is able to accurately distinguish the first three bending modes with more stable estimates and lower variance compared to the original KF-SSI algorithm and follows a similar trend compared to other approaches.

**KEYWORDS**
damping, harmonics, Kalman filter, offshore wind turbine, operational modal analysis, stochastic subspace identification

## 1 | INTRODUCTION

Operational modal analysis (OMA) is a widely used method for identifying the modal parameters of vibrating structures in operation. One of the main advantages of this approach is that it does not require knowledge of the excitation force, which can be difficult to obtain for large industrial structures. However, OMA is based on the assumption of stationary white noise excitation, which may not hold for certain applications, such as offshore wind turbines (OWTs). These structures are subjected to both random and harmonic loading due to the rotation of the rotor, which can make the application of conventional OMA techniques challenging. For example, structural modes may not be accurately identified or vibration caused by harmonics may be difficult to distinguish from vibrations at structural modes.[1]

Several methods have been developed to address the presence of harmonics in OMA. An elementary method involves recognizing harmonic components in response spectra as modes with zero damping.[1] This technique generally does not apply to OWTs as variations in rotor velocity

over a measurement length cause non-stationary harmonic components which appear as broader spectral peaks with apparent non-zero damping. Other techniques include modified classical algorithms, such as the modified least-squares complex exponential (LSCE) algorithm[1,2] and the modified Ibrahim time domain algorithm.[3,4] More classical algorithms have been similarly extended.[5–7] However, the effectiveness of these methods is ambiguous as exact knowledge of the harmonic frequency may be required to obtain accurate results, which can be difficult to achieve in practice.

Preprocessing techniques, such as time-synchronous averaging (TSA)[8,9] and Cepstrum editing,[10,11] have been proposed to filter out harmonics in experimental data. TSA is a popular method in gearbox modal analysis and is generally effective for stationary harmonics, but is less suitable for non-stationary harmonics. Order tracking,[12] a technique that removes the variability of harmonics and forces them to a single frequency, has been proposed as a solution for non-stationary harmonics, but this method averages the amplitude and does not fully remove variability, making it less practical as a preprocessor for modal analysis. Cepstrum editing, on the other hand, has been shown to be a suitable technique for non-stationary harmonics as long as sufficient harmonic multiples are present. However, it requires careful application, can affect the damping and can only remove periodic components that are uniformly spaced (including both harmonics and sidebands) and are hence more applicable to OWT gearbox OMA than for the modal analysis of the OWT support structure. Both TSA and Cepstrum editing have been applied to OWTs with inconclusive results. In some cases, TSA has been effective, while in others, it has not, possibly due to non-stationary harmonics. Cepstrum editing has also had mixed results, with some studies finding it to be effective and others not. In Manzato et al,[13] the frequency content was affected after applying Cepstrum editing, but the TSA approach yielded good results. On the other hand, in Manzato et al,[14] the results were not satisfying with TSA, most likely due to non-stationary harmonics, and a slightly different application of Cepstrum yielded good results. A recent survey paper discusses the current state of Cepstrum editing and modal analysis, highlighting the need for further research in this area.[15]

Other methods for dealing with harmonics in OMA involve the use of statistical indicators for harmonic localization, such as the probability density function (PDF),[16] kurtosis,[17,18] and entropy.[18] The effectiveness of these methods depends on the peakedness of the distribution of the harmonic component. Additionally, they may be of use as preprocessors for other algorithms.

A more recent category of algorithms is independent of the input spectrum and uses transmissibility functions, which contain modal information unaffected by harmonic excitation.[19] However, these approaches are not yet optimal for OMA of OWTs, as they have important limitations. For example, some methods require different loading conditions or multiple output sensors, making them impractical for certain applications.[19–21] Others require the acting forces to be uncorrelated,[22–24] which can be problematic when dealing with correlated harmonics induced by the turbine rotor.[25]

Recently, a novel approach called Kalman filter-based stochastic subspace identification (KF-SSI) was developed using the classical SSI algorithm[26] that involves state reconstruction using a Kalman filter and subsequent orthogonal removal of the harmonic subsignal from the original signal.[27] This method was reviewed together with other state-of-the-art OMA algorithms on applicability to operational OWTs in van Vondelen et al[28] and was rated favourably due to its effective harmonic mitigating properties. Although the method is promising, a full benchmarking of this algorithm for a realistic application with experimentally obtained data has not yet been performed. Further, practical issues such as numerical stability and the concatenation of multiple datasets for estimate refinement have not yet been investigated. In this paper, we, therefore, address these topics and present the following contributions:

1. We propose an extension to the KF-SSI method enabling numerically stable dataset concatenation for practical OMA applications.
2. We evaluate the proposed enhancement in (1) and the original KF-SSI method on an operational OWT, with a comparison of their performance.
3. We benchmark the results of (2) against those obtained using the current state-of-the-art OMA methods: modified LSCE and PolyMAX.
4. We evaluate preprocessor approaches for the (enhanced) KF-SSI method to accurately localize harmonics in the response data.

The next section introduces the field setup and describes the data acquisition. Section 3 presents the identification framework. Here, different methods for harmonic localization are compared, along with methods to improve identification results using KF-SSI. In Section 4, the results are analysed after applying the KF-SSI identification framework to a 6 MW operational OWT. This paper is concluded in Section 5.

## 2 | ACQUIRING DATA FROM AN OPERATIONAL WIND TURBINE

The International Electrotechnical Commission (IEC) 61400 standard specifies the sensor requirements of OWTs.[29] However, these sensors are often insufficient for performing modal analysis, as they are typically only installed at the top of the tower where the first-order mode exhibits the most deviation.[30] Capturing higher order modes requires additional sensors,[13] but this can be a costly endeavour. Ozbek and Rixen provide a comprehensive overview of different sensor configurations for OMA in OWTs.[31] In this paper, we aim to identify higher order modes in an economical setup with only two accelerometers. Note that while the first fore–aft (FA) and side–side (SS) mode shapes can be reconstructed using two accelerometers, reconstructing higher mode shapes requires at least three accelerometers. Mode shape reconstruction is therefore outside the scope of this paper.

The field measurements for this study were taken from a 6 MW Siemens Gamesa SWT-6.0-154 OWT at the Dudgeon wind farm located in the United Kingdom 32 km off the coast of Cromer. The site has a water depth between 18 and 25 m, an average wind speed of 9.8 m/s and a mean wave height of 1.1 m. The turbines have monopile foundations, a rotor diameter of 154 m and a hub height of 110 m. The layout of the wind farm is illustrated in Figure 1.

The Dudgeon wind farm utilizes advanced instrumentation in several of its turbines, including the use of bi-axial accelerometers on two levels. These sensors feature a high resolution of less than 0.001 g, a low non-linearity of 0.2% full scale in the range of ±3 g and minimal sensitivity to temperature changes of less than 0.05%/°C. These sensors are housed in protective enclosures and mounted on the internal walls of the turbine towers, as illustrated in Figure 2A. The sensors are placed optimally for modal analysis but are constrained by the mounting options on the tower. The yaw and rotor velocity measurements were also used for the identification procedure. The yaw signal measures the angular position of the rotor around the $z$ direction and was used to transform the $x$ and $y$ directions of the accelerometers to the rotor coordinate system, aligning them with the direction of the FA and SS bending modes (see Figure 2B). The generator rotational speed signal, which was measured by the turbine controller using an inductive sensor and interfaced to the data acquisition system, was used to determine the location of the harmonics.

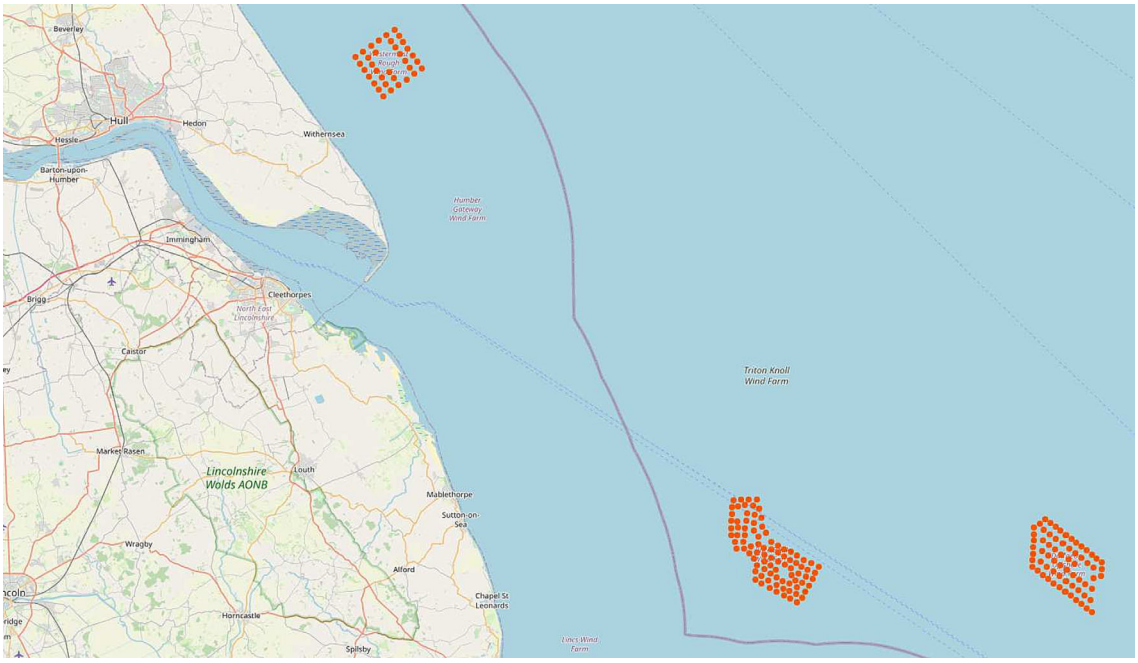


**FIGURE 1** Layout of the Dudgeon wind farm compared to other wind farms. From left to right: Westermost rough, Sheringham shoal, Dudgeon.

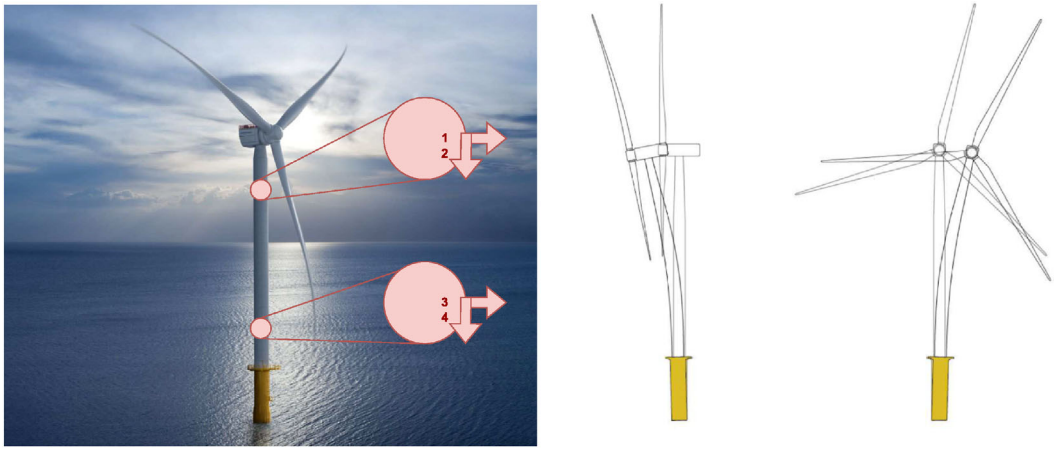


(A) Locations of the four accelerometers mounted on the tower of the Dudgeon Offshore Wind Turbine.

(B) Illustration of the first FA (left) and SS (right) bending modes.

**FIGURE 2** Illustrations of the sensors and first tower bending modes.

The datasets were sampled at a rate of 25 Hz, enabling the reconstruction of vibrations up to 12.5 Hz. This frequency range captures all main modes and harmonics. For confidentiality reasons, all results have been normalized to fall between 0 and 1. The data were collected in 10-min batches, which can provide good estimates of the modal parameters. Even better results can be obtained by concatenating datasets as long as they are stationary and have similar environmental conditions. However, this procedure is not trivial and will be detailed further in Section 3.2.

## 3 | IDENTIFICATION FRAMEWORK

This section presents the steps for identifying the modal parameters of a 6 MW OWT using the KF-SSI method, as illustrated in Figure 3. The approach is adapted from the work of Greś et al. for this specific application. Thus, only the proposed enhancements are discussed in this section and the reader is referred to Greś et al[27] for the other steps in the framework.

### 3.1 | Localizing the harmonics

Harmonics in data can often hide the underlying system dynamics or reduce identification accuracy in OMA algorithms. To remove harmonics using the KF-SSI algorithm, it is necessary to determine their frequency location. The kurtosis indicator, suggested as a preprocessor for KF-SSI,[27] has been used to distinguish harmonics from structural modes (e.g., Jacobsen et al.[34]). As the effectiveness of this method may be limited for non-stationary harmonics, it is investigated in this section whether this approach is suitable for OWT response data. The method is evaluated on a simple three-degree-of-freedom system with known system dynamics, after which it is tested on OWT field data with unknown dynamics. The results are compared against two other approaches: the entropy approach, as used in Agneni et al[18] and the rotor velocity method as suggested in, for example, Manzato et al.[35] Note that the rotor velocity method only applies to systems where the rotating components causing the disturbing harmonics are measured (i.e., helicopter and OWT). The best-suited approach for an OWT will be selected to localize the harmonics in the KF-SSI framework. First, the three-degree-of-freedom system is introduced in the next section.

#### 3.1.1 | Acquiring data from a three-degree-of-freedom system

In this section, a three-degree-of-freedom system is derived and simulated. The system is composed of masses $m_i$, springs $k_i$ and dampers $c_i$ for $i = 1,2,3$, as illustrated in Figure 4. Each mass is connected to the next mass using one spring and one damper. The first mass is connected to a fixed frame, and the last mass is free.

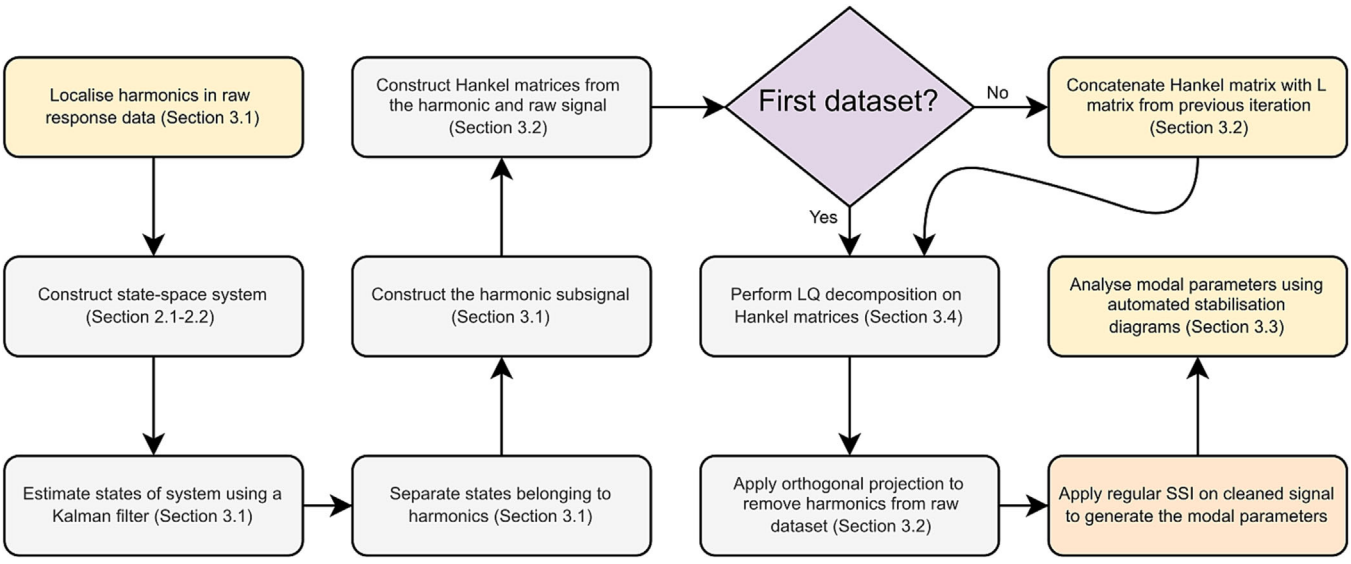


**FIGURE 3** Overview of the identification framework used in this study. The yellow boxes are the steps presented in this work, indicated with the respective sections. The grey boxes are the steps presented in the work of Greś et al,[27] indicated similarly with their sections. The orange box refers to an SSI method as can be found in, for example, Verhaegen[32] and Van Overschee and De Moor.[33]

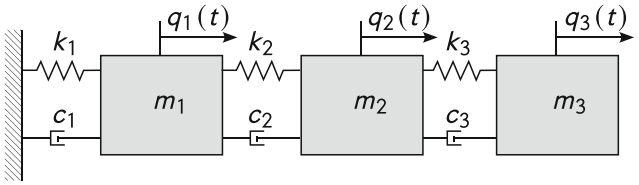


**FIGURE 4** Schematic of the three-degree-of-freedom system where $m_i$, $k_i$ and $c_i$ for $i = 1,2,3$ are the mass, stiffness and damping, respectively.

A force $f(t) \in \mathbb{R}^3$ excites the system at each degree of freedom. The equations of motion are

$$M\ddot{q}(t) + J\dot{q}(t) + Kq(t) = f(t), \tag{1}$$

with

$$M = \begin{bmatrix} m_1 & 0 & 0 \\ 0 & m_2 & 0 \\ 0 & 0 & m_3 \end{bmatrix}, J = \begin{bmatrix} c_1 + c_2 & -c_2 & 0 \\ -c_2 & c_2 + c_3 & -c_3 \\ 0 & -c_2 & c_3 \end{bmatrix}, K = \begin{bmatrix} k_1 + k_2 & -k_2 & 0 \\ -k_2 & k_2 + k_3 & -k_3 \\ 0 & -k_2 & k_3 \end{bmatrix},$$

where $M \in \mathbb{R}^{3\times3}$ is the mass matrix, $J \in \mathbb{R}^{3\times3}$ is the damping matrix, $K \in \mathbb{R}^{3\times3}$ is the stiffness matrix and $\ddot{q}(t), \dot{q}(t), q(t) \in \mathbb{R}^3$ are the vectors of acceleration, velocity and position in the generalized coordinate system, respectively. By defining the state vector and input vector as

$$x(t) = \begin{Bmatrix} q(t) \\ \dot{q}(t) \end{Bmatrix} \in \mathbb{R}^6, \quad u(t) = f(t) \in \mathbb{R}^3, \tag{2}$$

the following state-space model is obtained:

$$\begin{aligned} \dot{x}(t) &= \underbrace{\begin{bmatrix} 0 & I \\ -M^{-1}K & -M^{-1}J \end{bmatrix}}_{A} x(t) + \underbrace{\begin{bmatrix} 0 \\ M^{-1} \end{bmatrix}}_{B} u(t), \\ &= Ax(t) + Bu(t), \end{aligned} \tag{3}$$

where $A \in \mathbb{R}^{6\times6}, B \in \mathbb{R}^{6\times3}$. The system of Equation (3) can be observed through sensors at three degrees of freedom that capture the displacement $q(t)$, velocity $\dot{q}(t)$ or acceleration $\ddot{q}(t)$ and are collected in a vector $y(t) \in \mathbb{R}^3$ as follows:

$$y(t) = C^{\text{acc}}\ddot{q}(t) + C^{\text{vel}}\dot{q}(t) + C^{\text{dis}}q(t), \tag{4}$$

where $C^{\text{acc}}, C^{\text{vel}}$ and $C^{\text{dis}} \in \mathbb{R}^{3\times3}$ are the output location matrices for acceleration, velocity and displacement, respectively. The system will only be observed at the accelerations, per the actual measurement data of the OWT. Therefore, the following observation equation is obtained:

$$\begin{aligned} y(t) &= \underbrace{\begin{bmatrix} -C^{\text{acc}}M^{-1}K & -C^{\text{acc}}M^{-1}J \end{bmatrix}}_{C} x(t) + \underbrace{C^{\text{acc}}M^{-1}}_{D} u(t), \\ &= Cx(t) + Du(t), \end{aligned} \tag{5}$$

where $C \in \mathbb{R}^{3\times6}$ and $D \in \mathbb{R}^{3\times3}$. Equations (3) and (5) define the state-space model in continuous time.

The parameters of the $M$, $J$ and $K$ matrices are chosen such that they yield the modal parameters as given in Table 1a. Response data were generated by exciting the system at all frequencies using zero-mean Gaussian white noise, and additional harmonics are included in the identification signal to simulate the effect of the OWT harmonic loading. Noise is added to the output signal to achieve a signal-to-noise ratio of 80 dB, simulating measurement noise. The frequencies of these harmonics are displayed in Table 1b. The system is sampled at a rate of 25 Hz and in 10-min intervals, similar to the OWT data. In the next section, these datasets and the datasets obtained from the Dudgeon offshore wind farm will be analysed with harmonic localization methods to estimate the harmonic frequencies as a preprocessor for KF-SSI.

**TABLE 1** Overview of the parameters used for the three-degree-of-freedom simulation.

| Mode | Nat. freq. (Hz) | Damping ($\delta$ %) | Harmonic | Freq. (Hz) |
|---|---|---|---|---|
| (a) Structural modes | | | (b) Harmonics | |
| 1 | 0.5008 | 19.87 | 1P | 0.781 |
| 2 | 1.4033 | 31.26 | 2P | 1.562 |
| 3 | 2.0279 | 42.49 | 3P | 2.343 |
| | | | 4P | 3.124 |
| | | | 5P | 3.905 |
| | | | 6P | 4.686 |
| | | | 7P | 5.467 |

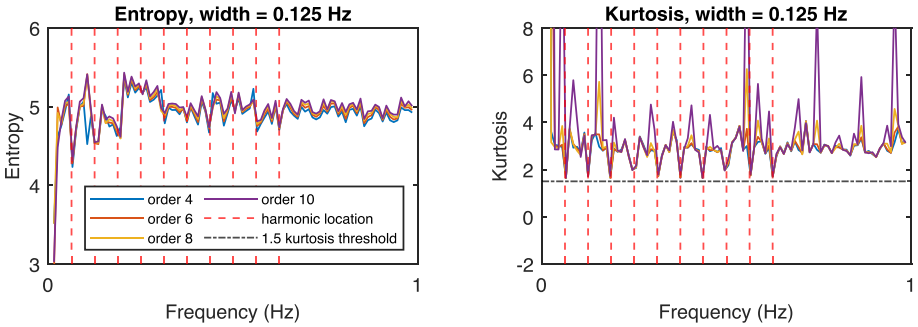


**FIGURE 5** Comparison of the kurtosis and entropy statistical indicator for different filter orders on a simple three-degree-of-freedom system with 10 harmonics.

### 3.1.2 | Harmonic localization using statistical indicators

This section will evaluate statistical indicators, kurtosis and entropy, for harmonic localization in KF-SSI on three-degree-of-freedom system response data and field data. These indicators rely on the properties of the distribution of the signal to determine the location of harmonics.

Kurtosis is a measure of the peakedness of a distribution. It can be computed at each frequency of the response signal by shifting a narrow bandpass filter over the entire frequency band of interest. For a signal that has a standard normal distribution, this computation yields a value of $\gamma = 3$. For harmonic signals that consist of sinusoids with zero mean $\mu$ and unit variance $\sigma^2$, the kurtosis value is $\gamma \approx 1.5$. By comparing the kurtosis values at different frequencies, it is possible to distinguish between the two types of distributions.

Entropy is a measure of the randomness or uncertainty of a distribution. It attains a zero value if and only if the occurrence of a value is certain and has a positive value otherwise. This property can be exploited to distinguish deterministic signals, such as harmonics, from stochastic processes. The entropy value is non-maximum in regions of deterministic components and maximum in regions of stochastic components.

*Evaluation on the three-degree-of-freedom system*

Here, the kurtosis and entropy statistical indicators have been evaluated on simulation data of a simple three-degree-of-freedom system illustrated in Figure 4. Each signal is bandpass filtered by passing a Butterworth filter over the entire frequency after which the statistical indicator is applied. Figure 5 displays the results, where the vertical dashed red lines indicate the harmonics. In this figure, the indicators are compared for different filter orders. It can be observed that the local minima in the entropy plot indicate the harmonic locations. However, other local minima can be observed that do not indicate a harmonic, complicating localization without prior knowledge. In the kurtosis plot, the results are accurate for all harmonics, as the kurtosis value attains 1.5 at each harmonic frequency. These results indicate that statistical indicators can be suitable as a preprocessor for KF-SSI with data from the three-degree-of-freedom system. Next, it will be investigated if this also holds for OWT field data.

*Evaluation on OWT field data*

Here, the kurtosis and entropy statistical indicators have been evaluated on field data acquired from the Dudgeon offshore wind farm as described in Section 2. Remarkably, both indicators show poor performance, as can be seen in Figure 6. The 1P, 3P, 6P, 9P and 12P harmonics are indicated by the red dashed lines, where P denotes the rotor period. In the entropy plots, there is no consistent correspondence to the expected harmonics visible in the local minima of the entropy plots. Similarly, the kurtosis does not reach the expected value of 1.5 at the locations of the harmonics.

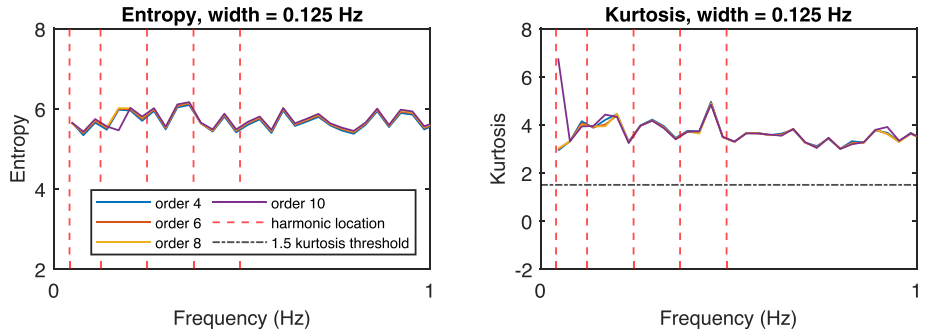


**FIGURE 6** Comparison of the kurtosis and entropy statistical indicator for different filter orders on a field-measured dataset.

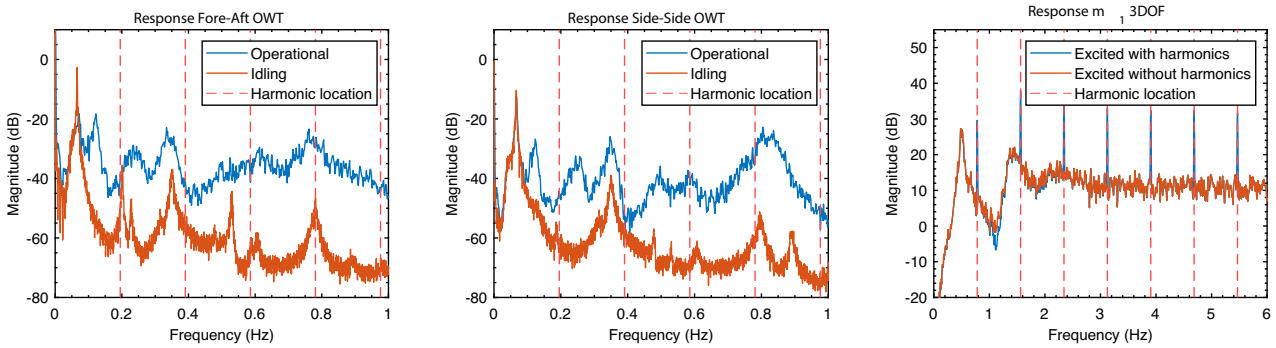


**FIGURE 7** Comparison of the response spectra of the tower sensors using idling-only and operational data against the response spectrum of the first mass $m_1$ of the three-degree-of-freedom system, excited with and without harmonics. Note that the harmonics are much broader in the OWT response spectra compared to the three-degree-of-freedom system.

The poor performance of the identification method might be attributed to the broader, non-stationary, harmonic peaks in the response spectra of field data from an OWT. These peaks are not as sharp as the peaks caused by the ideal harmonics in the response of the three-degree-of-freedom system, as shown in Figure 7. In essence, due to the continuously varying rotor speed in OWT data, a 'harmonic' is no longer a discrete frequency in the time domain, although it would be uniquely identifiable as such in the angle domain. As a result, a more comprehensive filter might be required to capture the entire harmonic signal. However, using a wider filter could result in less accurate localization of the harmonic and undermine its effectiveness. In a subsequent experiment, large filter widths were tried, but this did not improve the localization of the harmonics.

These results suggest that neither indicator is effective in identifying the harmonics in the field data of an OWT and also shed light on the reason classical OMA methods combined with such harmonic localization techniques often do not yield sufficiently good results. On the other hand, a periodic component estimator, as used by KF-SSI, identifies both the varying amplitude and the frequency of the harmonic component and may be considered more suitable for the application of OWT OMA. The next section will investigate an alternative method for localizing harmonics.

### 3.1.3 | Harmonic localization using the rotor velocity signal

In this section, it is investigated whether the rotor velocity signal can be used as a suitable indicator for harmonics in response data. In OWT measurements, the rotor velocity is generally available. This signal could be suitable for harmonic localization but it is not constant over time. Therefore, the mean value over the entire sample (of 10 min) was used as an estimate of the base frequency of the rotor and its harmonics. This method is most effective for rotational velocities that are approximately stationary, as the harmonic peak will be concentrated around a single frequency value. If the rotational velocity is less stationary, the peak will be less sharp, and the estimation accuracy might decline, making this method less interesting.

Field data from an OWT grid drop event were used to determine the accuracy of this method. During a grid drop event, the power of the turbine quickly drops to zero, causing a massive thrust impulse to the OWT and setting up long-lasting oscillations in the tower. The speed reduction also causes a decrease in damping, leading to longer lasting oscillations. The turbine then enters an 'idling' state, where no electricity is generated. While the turbine tower is still vibrating from its previous operational state and is excited by wind and wave loading, the acceleration sensors only measure the tower's response to these external loads and no longer capture the periodic loading caused by the rotor.

When comparing the time series from both states, idling and operational, different response spectra are found. In Figure 7, the red vertical dashed lines indicate the harmonics 1P, 3P, 6P, 9P and 12P estimated based on the rotational velocity. These lines agree with distinct peaks in the spectrum of the full time series, where the operational state is considered. When inspecting the response spectrum of the idling state, the indicated peaks have vanished, which suggests that they are associated with harmonics. Several modes that were clouded by the harmonics also become visible now.

According to the above analysis, the rotor velocity method is effective in identifying the locations of harmonics in an operational OWT. As a result, it was chosen for use in the identification framework of Figure 3 over the statistical methods. The next steps in the framework are conducted following the methodology described in Greś et al.[27] The novel enhancement of the algorithm, which entails modal analysis estimate refinement with additional data, is presented in the next section.

## 3.2 | OMA estimate refinement: concatenating multiple datasets

In this section, the authors propose a data concatenation step to enhance the performance of the KF-SSI algorithm. Conventionally, when additional data becomes available, OMA estimate refinement is performed by treating the new data as an independent dataset, and then performing statistical averaging of old and new modal parameter estimates. However, this approach may lead to biased results: Even if the underlying system excitation is zero-mean white noise, the modal parameter estimates based on finite-length datasets are not normally distributed, and statistical averaging may hence not converge to unbiased modal parameter estimates.

For unbiased OMA estimation, concatenation of datasets has hence been proposed and investigated in the current paper. Using more data may improve the estimated values, but care must be taken when combining multiple distinct datasets. For wind turbines, where the dynamics change with wind speed, it may be required to assemble multiple datasets from distinct periods where the environmental and operational conditions were found to be similar to ensure accurate results. However, simply combining datasets without addressing the state mismatch between the final entry of the first data sequence and the first entry of the second data sequence could yield incorrect results. In the following, a method is proposed to mitigate the effects of the state mismatch and improve the overall accuracy of the identification process.

The KF-SSI algorithm can be efficiently and accurately implemented using an LQ decomposition as described in Section 3.4 of the paper by Greś et al. This decomposition can also be leveraged to effectively concatenate multiple datasets without introducing state inconsistencies.[36,37] The results obtained from this concatenation step are hereafter referred to as enhanced KF-SSI, and they are compared to the standard KF-SSI algorithm without concatenation in Section 4.2. The following theorem, similar to the method presented in Döhler and Mevel,[36] illustrates this concept in detail.

**Theorem 1.** *Any matrix $G \in \mathbb{R}^{m\times n}$, can be decomposed as follows*[38]*:*

$$G = LQ^T, \tag{6}$$

*where $L \in \mathbb{R}^{m\times n}$ is a lower triangular matrix with zeros added as rows or columns if $m > n$ or $n > m$, respectively, and $Q \in \mathbb{R}^{n\times n}$ is an orthogonal matrix. Let $Y \in \mathbb{R}^{m\times n}$ be a data matrix and split into two matrices $Y_1$ and $Y_2$ yielding the following decomposition:*

$$[Y_1 \;\; Y_2] = LQ^T. \tag{7}$$

*Alternatively, $Y_1$ can first be decomposed as*

$$Y_1 = L_1 Q_1^T, \tag{8}$$

*and matrix $L_1$ can be used in the following decomposition instead of matrix $Y_1$:*

$$[L_1 \;\; Y_2] = LQ_\star^T, \tag{9}$$

*yielding the same L matrix but a different orthogonal matrix $Q_\star$.*

*Proof of Theorem* 1. See Appendix A. ∎

The above theorem highlights the key difference between the two methods for LQ decomposition, as represented by Equation (7) and Equations (8) and (9). The former requires state continuity between matrices $Y_1$ and $Y_2$, while the latter does not. This means that by using the latter method, it is possible to concatenate datasets without regard to state continuity. However, note that while the resulting L matrix is the same in both cases, the Q matrix may be different depending on the concatenation method used. This concept can be leveraged to improve the accuracy of the

identification process and be directly applied to the KF-SSI algorithm from Greś et al,[27] by substituting $Y$ for $\begin{bmatrix} Y_{per}^T & Y_{raw}^T \end{bmatrix}^T$, where $Y_{per}$ is a Hankel matrix containing the estimated periodic subsignal and $Y_{raw}$ is a Hankel matrix containing the measured raw dataset, per terminology of Greś et al.

Following this, the next steps of the identification framework are carried out according to the methodology outlined in Greś et al.[27] The final is elaborated in the next section.

## 3.3 | Interpreting identification results

This section describes how the identification results were analysed. The damping discussed in this paper is modal damping, a form of damping specific to a structure's natural modes of vibration. It is represented by the logarithmic decrement, $\delta$, which is a standard measure of damping in the wind energy industry.[29] It is related to the damping ratio, $\zeta$, which is the percentage of critical damping, and for small values can be approximated as $\delta \approx 2\pi\zeta$. The output of OMA is typically collected in 'stabilization diagrams', which enable the determination of the stable natural frequencies and damping of the system. This diagram is constructed by repeating the same OMA procedure using different assumed system orders. The identified modes are plotted vertically across a power spectrum of the response signal, starting with a low system order. As the system order increases, the modes should be persistently found across multiple orders, indicating that they are stable (see, e.g., Figure 9).

Analysing multiple datasets using the stabilization diagram can be a cumbersome task. Several approaches exist to avoid the need for this manual analysis, with varying levels of complexity. An elaborate description of some of these approaches can be found in the work of Reynders et al.[39] The current study employs a simple heuristic method for automatic interpretation. Since the optimal identification order is unknown, OMA was applied to the same dataset multiple times using a range of orders yielding mode estimates. The goal is to determine the optimal identification order yielding all desired structural modes. However, only a subset of the modes identified are actual modes of vibration, which is generally assumed if they are persistently found across multiple orders. Other identified modes might be spurious, while it is also possible that some modes may not be identified at certain orders. Therefore, the minimum order should be found at which the maximum number of persistent modes could be identified. The modes identified at this order should then be used in the analysis. A pseudo -code is given below:

**Algorithm 1** Automatic interpretation stabilization diagram

1: Choose a range of orders for which to perform OMA on a dataset.
2: **for** each identification order **do**
3: Estimate the modes using OMA on the dataset.
4: **end for**
5: Select only the persistent modes that are found at multiple orders (e.g., 3–5 orders) and discard the others.
6: **for** each identification order **do**
7: Count how many persistent modes are found at each order.
8: **end for**
9: Determine which identification order contains the most persistent modes.
10: **if** multiple orders have the highest number **then**
11: Select the lowest order containing them.
12: **end if**
13: Use the persistent modes identified at this order as the analysis result.

*Note that a user-defined tolerance needs to be permitted for Steps 5, 7 and 9 to accommodate estimation variance.*

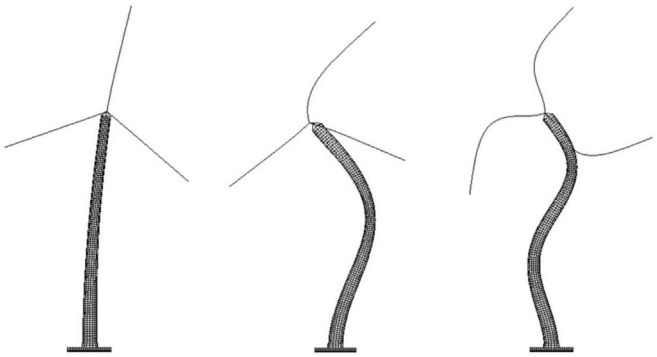

**FIGURE 8** Illustration of the first three SS tower bending modes of a wind turbine, where left is the first, middle is the second and right is the third mode. Figure adapted from Fernández Fernández et al.[40]

## 4 | APPLICATION TO AN OPERATIONAL OWT

This section aims to estimate the modal damping and natural frequencies of a 6 MW OWT using the framework outlined in Figure 3. To accomplish this, 10 distinct datasets were analysed at various wind speeds ranging from 5 to 26 m/s. The goal is to determine the natural frequency and

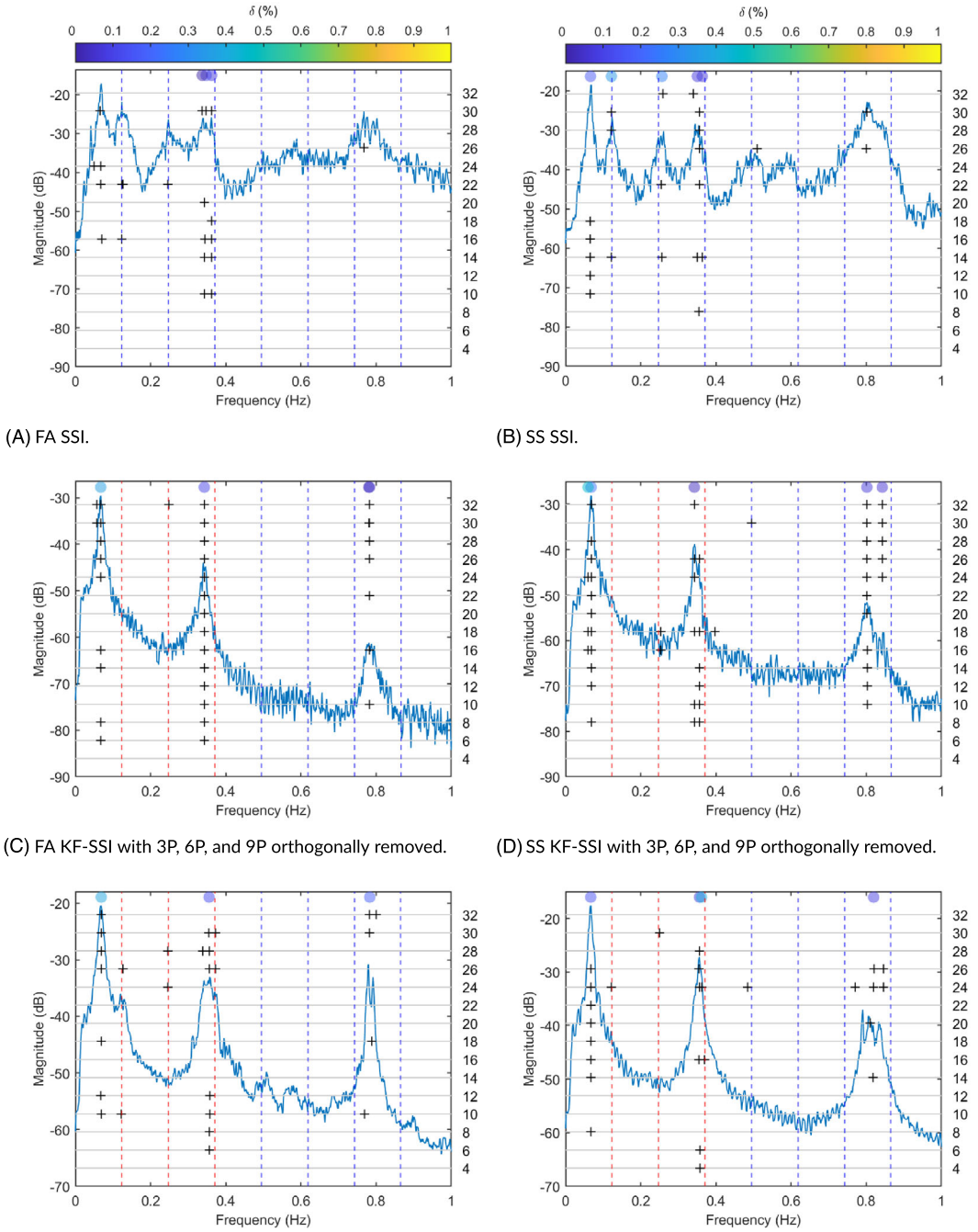


(A) FA SSI. (B) SS SSI.

(C) FA KF-SSI with 3P, 6P, and 9P orthogonally removed. (D) SS KF-SSI with 3P, 6P, and 9P orthogonally removed.

(E) FA Enhanced KF-SSI using 10 datasets with 3P, 6P, and 9P orthogonally removed. Note that the spectrum presented here is illustrative as it cannot be reconstructed (see text).

(F) SS Enhanced KF-SSI using 10 datasets with 3P, 6P, and 9P orthogonally removed. Note that the spectrum presented here is illustrative as it cannot be reconstructed (see text).

**FIGURE 9** Comparison of the stabilization diagrams constructed from the results of the field data experiment using different settings of the KF-SSI algorithm for the FA and SS direction. The red dashed lines indicate the harmonics that were orthogonally removed and the blue dashed lines the harmonics that were not removed. Each stable mode is indicated by a '+' and corresponds to the order as indicated by the right axis.

damping of the first three tower bending modes in both the FA and SS directions (as depicted in Figure 8). The following section will use this framework to generate a single estimate, while Section 3.2 will use it to generate multiple estimates at all available wind speeds.

### 4.1 | Single estimate from field measurements

To evaluate the enhanced KF-SSI framework and produce a single estimate for each mode, ten datasets at an above-rated wind speed of 13 m/s were used to generate an estimate of the modal parameters. For qualitative comparison, these results were then compared to the results of classical KF-SSI and SSI using only a single dataset. The 3P, 6P and 9P harmonics were removed using the (enhanced) KF-SSI algorithms but remained in the response signal when using the SSI method. Stabilization diagrams were then generated for analysis and displayed in Figure 9.

The coloured dots at the top of the figure indicate the modal damping in logarithmic decrement notation, and the red and blue dashed lines represent the harmonic locations. A red dashed line indicates that a harmonic has been removed, while a blue dashed line indicates that it has not been removed. Each stable mode is indicated by a '+' corresponding to the identification order indicated on the right axis.

A clear difference can be observed when comparing the power spectra in the stabilization diagrams of SSI and KF-SSI. Several peaks indicated by the red dashed lines, which represent the harmonics 3P, 6P and 9P, have vanished. Although the SSI algorithm was able to identify the first mode at several orders, the presence of the 3P harmonic can still affect the estimated modal parameters.[27] Also, note the identification of several harmonics. Removing the 3P harmonic allows for easier identification across multiple orders, as can be seen in the KF-SSI plots.

In the SSI stabilization diagram, observe that the 9P harmonic is directly on top of the second mode, which can be problematic for classical OMA algorithms to identify damping. The SSI algorithm does provide an estimate, but it is likely contaminated by the damping of the 9P harmonic due to their close proximity and the lack of an additional mode separating the two damping values. Removing the 9P harmonic with KF-SSI allows for a more accurate estimation of the second mode, as shown in the KF-SSI stabilization diagram. This diagram clearly displays the results for the second mode, and the removal of the harmonic also allows for estimates of the third bending mode around 0.8 Hz.

All three modes were also identified by the enhanced KF-SSI. However, unlike with regular KF-SSI, it is not possible to reconstruct the edited time signal from the Hankel matrices of the LQ decomposition due to the different $Q$ matrix (see Theorem 1). Therefore, the power spectra in Figure 9E,F, which are normally created from the edited time signal using regular KF-SSI, were constructed by averaging the individual power spectra obtained from each dataset after separate LQ decompositions. Also, note that the removal of the harmonic subsignal may reduce the amplitude of the reconstructed resultant signal but does not change the characteristics of the modal parameters. The estimated modal parameters are also given in Tables 2 and 3. This is a notable improvement over the estimation of SSI, as the KF-SSI and newly presented enhanced KF-SSI allow for the removal of harmonic components, yielding clearer stabilization diagrams. The next section will provide a more in-depth comparison between KF-SSI and enhanced KF-SSI for generating multiple estimates from field measurements, highlighting the variance reduction property of enhanced KF-SSI.

**TABLE 2** Comparison of the modal parameters obtained in the field data experiment for KF-SSI for the FA direction.

| | Natural frequency (Hz) | | | Damping ($\delta$ %) | | |
|---|---|---|---|---|---|---|
| Mode | Classical | KF-SSI | Enhanced | Classical | KF-SSI | Enhanced |
| 1 | - | 0.0673 | 0.0685 | 0.500 | 0.369 | 0.394 |
| 2 | 0.348 | 0.343 | 0.355 | 0.129 | 0.114 | 0.143 |
| 3 | - | 0.782 | 0.783 | - | 0.067 | 0.193 |

**TABLE 3** Comparison of the modal parameters obtained in the field data experiment for KF-SSI for the SS direction.

| | Natural frequency (Hz) | | | Damping ($\delta$ %) | | |
|---|---|---|---|---|---|---|
| Mode | Classical | KF-SSI | Enhanced | Classical | KF-SSI | Enhanced |
| 1 | 0.0663 | 0.0679 | 0.0669 | 0.173 | 0.236 | 0.145 |
| 2 | 0.351 | 0.343 | 0.356 | 0.0889 | 0.0391 | 0.0930 |
| 3 | - | 0.801 | 0.820 | - | 0.0775 | 0.0996 |

Abbreviations: Classical, classical stochastic subspace identification; Enhanced, enhanced Kalman filter-based stochastic subspace identification; KF-SSI, Kalman filter-based stochastic subspace identification.

## 4.2 | Multiple estimates from field measurements

In this section, the KF-SSI and enhanced KF-SSI algorithms were applied to multiple datasets. The box plots of the FA and SS directions are shown in Figures 10 and 11. The leave-one-out methodology was used to generate 10 different estimates for the enhanced KF-SSI algorithm using the

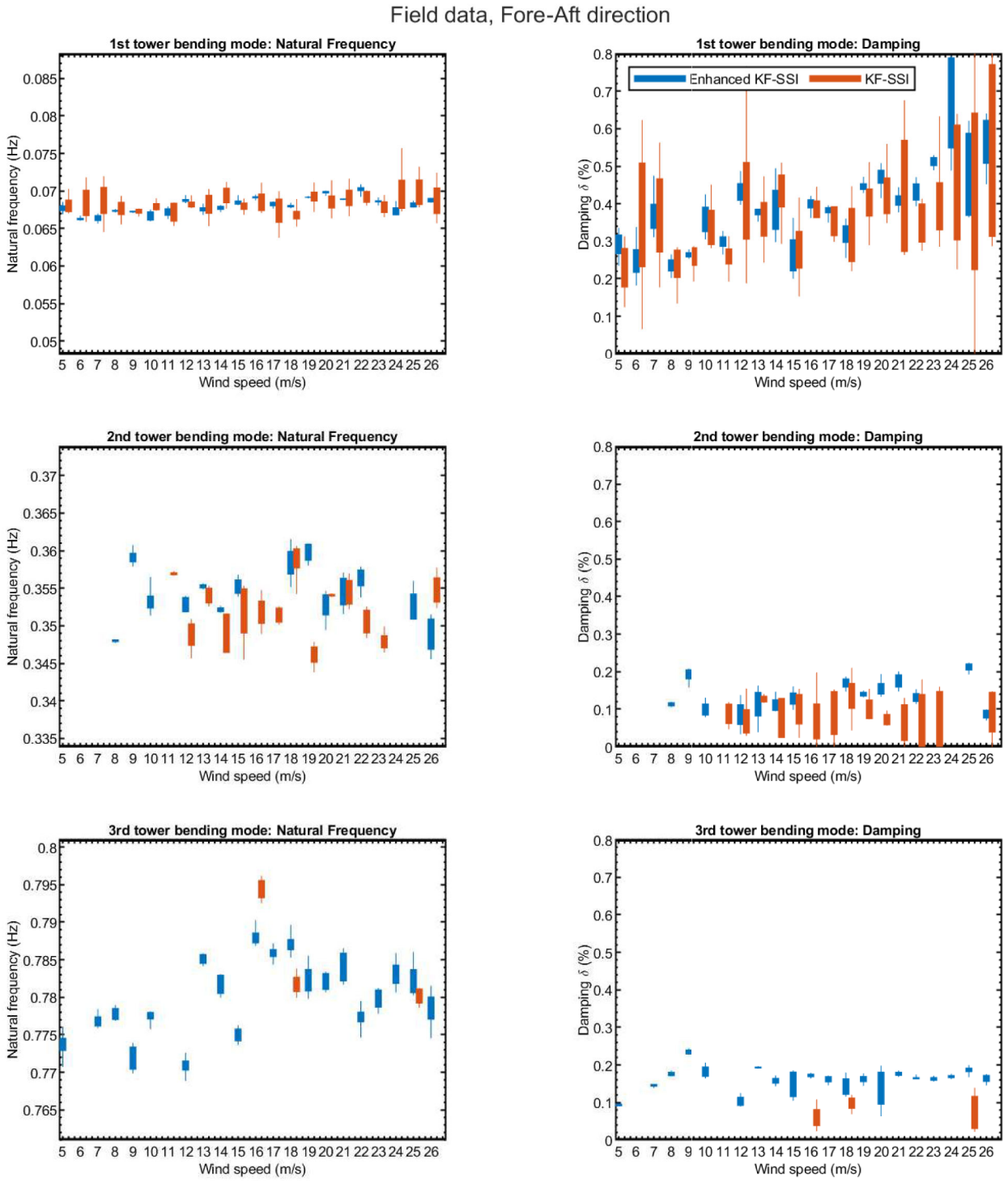


**FIGURE 10** Comparison of enhanced KF-SSI against original KF-SSI. Note that with enhanced KF-SSI, the mean is more stable, and estimate variance is lowered. Also, note that the axis limits of the natural frequency plots have a fixed 0.02 Hz upper and lower bound around the median estimate, and the axes of the damping plots have been fixed to 0.8 $\delta\%$ to visually compare the variance between the modes.

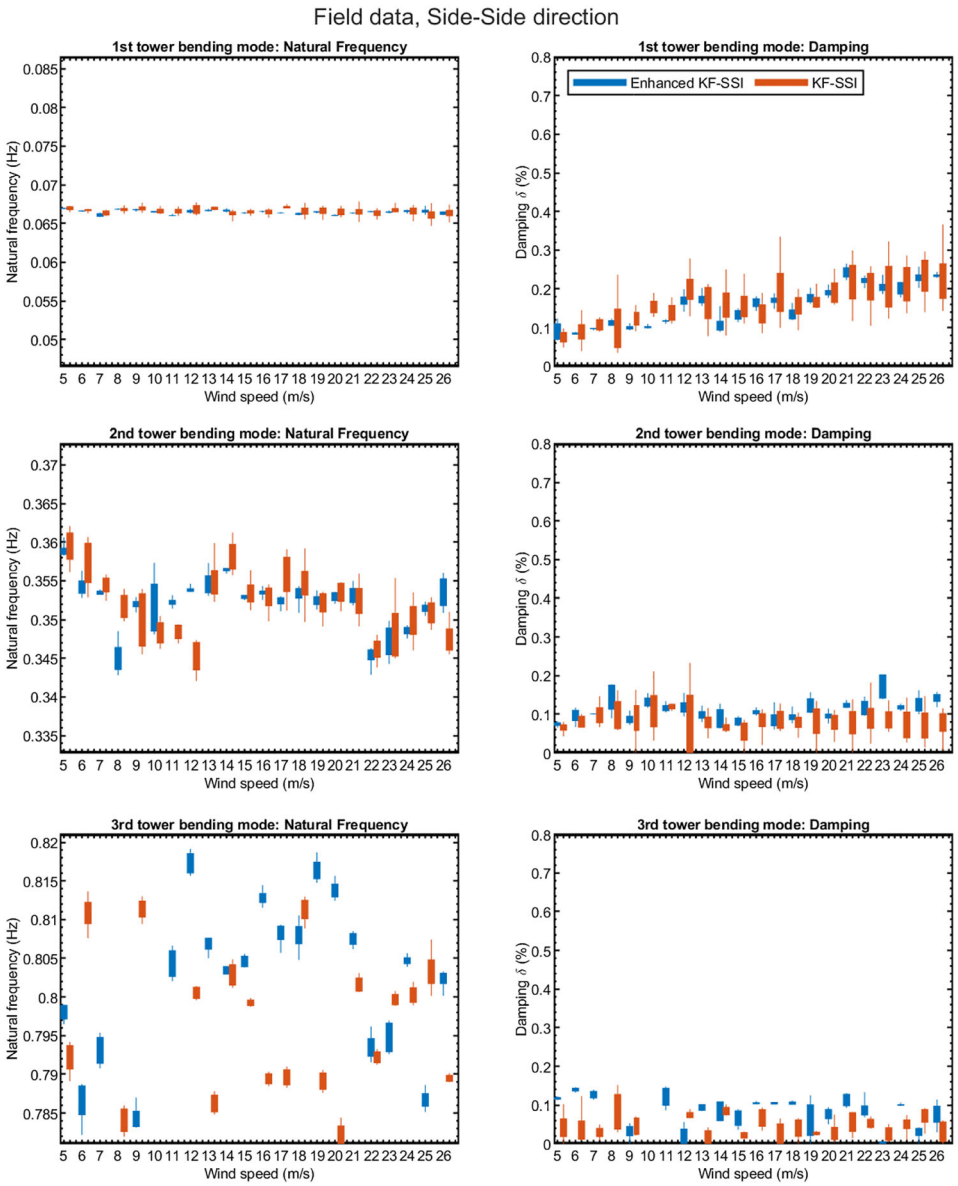


**FIGURE 11** Comparison of enhanced KF-SSI against original KF-SSI. Note that with enhanced KF-SSI, the mean is more stable, and estimate variance is lowered. Also, note that the axis limits of the natural frequency plots have a fixed 0.02 Hz upper and lower bound around the median estimate, and the axes of the damping plots have been fixed to 0.8 $\delta\%$ to visually compare the variance between the modes.

same 10 datasets in each estimation, while the original KF-SSI algorithm used only one dataset for each estimation. The enhanced KF-SSI algorithm exhibits a notable reduction in variance compared to the original algorithm, resulting in a significant improvement in identification precision. Both algorithms consistently identify the first mode, but the estimated natural frequencies and damping values for the second and third modes have larger variance, particularly for the original KF-SSI algorithm. The damping of the first mode increases with wind speed due to the increased effect of aerodynamic damping at higher speeds. Also, observe the large uncertainty around these estimates; the first FA mode damping is much more difficult to quantify precisely due to the high damping level. Free-decay experiments may provide more precise estimates.[41,42] However, the damping level heavily relies on operational conditions, making this method less suitable for operational damping estimation. The damping of the second and third modes remains approximately constant across all wind speeds.

Manual analysis of the 220 datasets could potentially improve the results further, but it is a time-consuming process. It is also worth noting that processing concatenated datasets requires additional computational resources compared to processing single datasets. While the data processing in this study was generally completed within a few minutes, this may not be feasible for applications with limited computation time available.

### 4.3 | Comparison against other algorithms

To benchmark the identification precision of enhanced KF-SSI, the results are compared against two other algorithms. The first is PolyMAX, a well-established frequency-domain OMA algorithm.[43] It is favoured due to its fast convergence and clear stabilization diagrams but does not include harmonics-mitigating steps in its identification procedure, so false modes may be identified without careful mode selection. The second

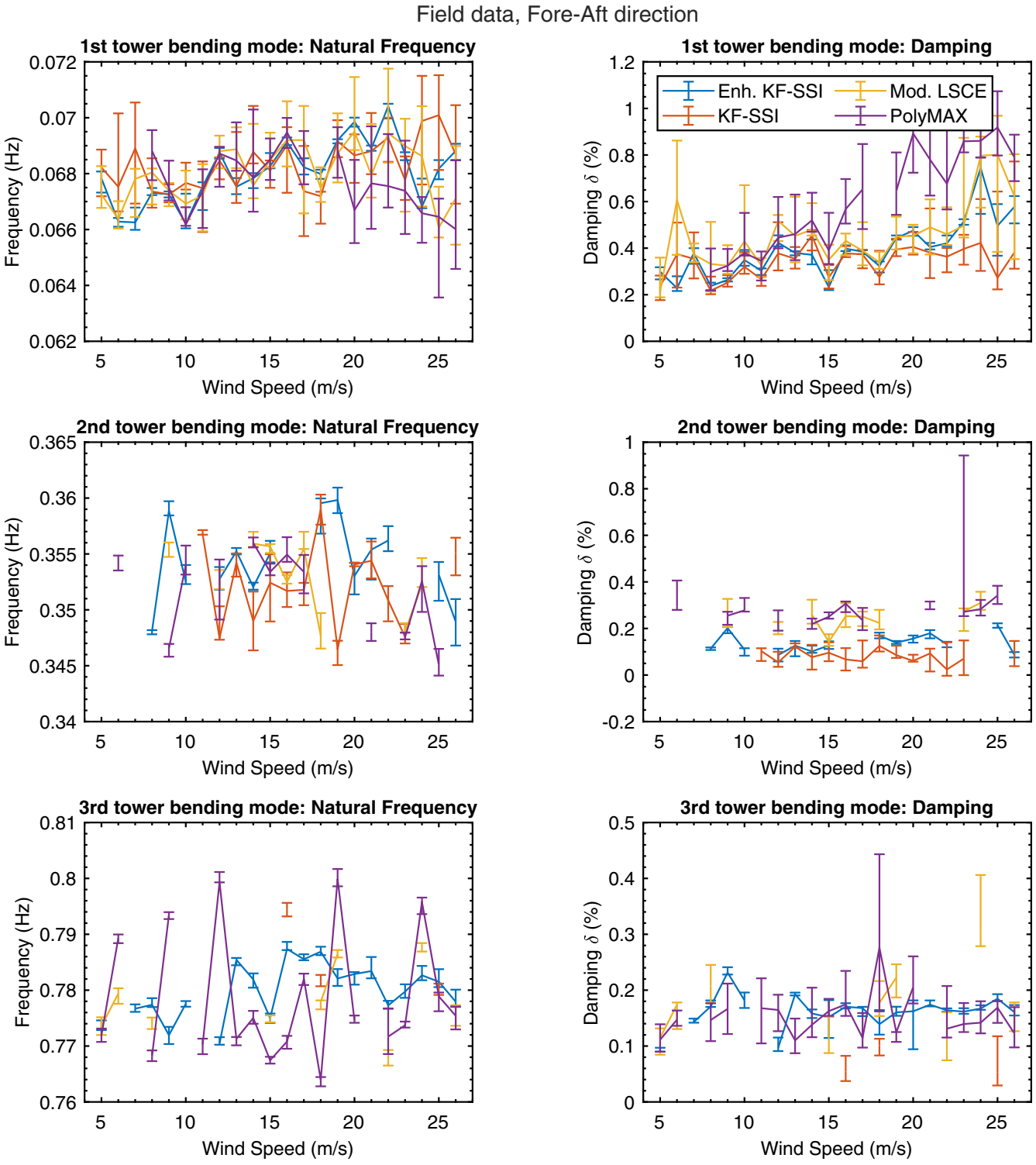


**FIGURE 12** Comparison of the estimation results of enhanced KF-SSI against PolyMAX and modified LSCE for the wind speed range. Median and variance values are given in Tables 4 to 7.

algorithm is the modified LSCE algorithm which incorporates the harmonics in the identification steps and uses the same a priori information as enhanced KF-SSI based on rotational velocity.[1]

A comparison of the median, first and third quantiles of each algorithm was performed on the same datasets as in the previous section. The resulting box plots are displayed in Figures 12 and 13, and the median values are listed in Tables 4 to 7. The enhanced KF-SSI algorithm stands out for its small variance compared to the other algorithms, and its median values match those of the other algorithms well. Additionally, the

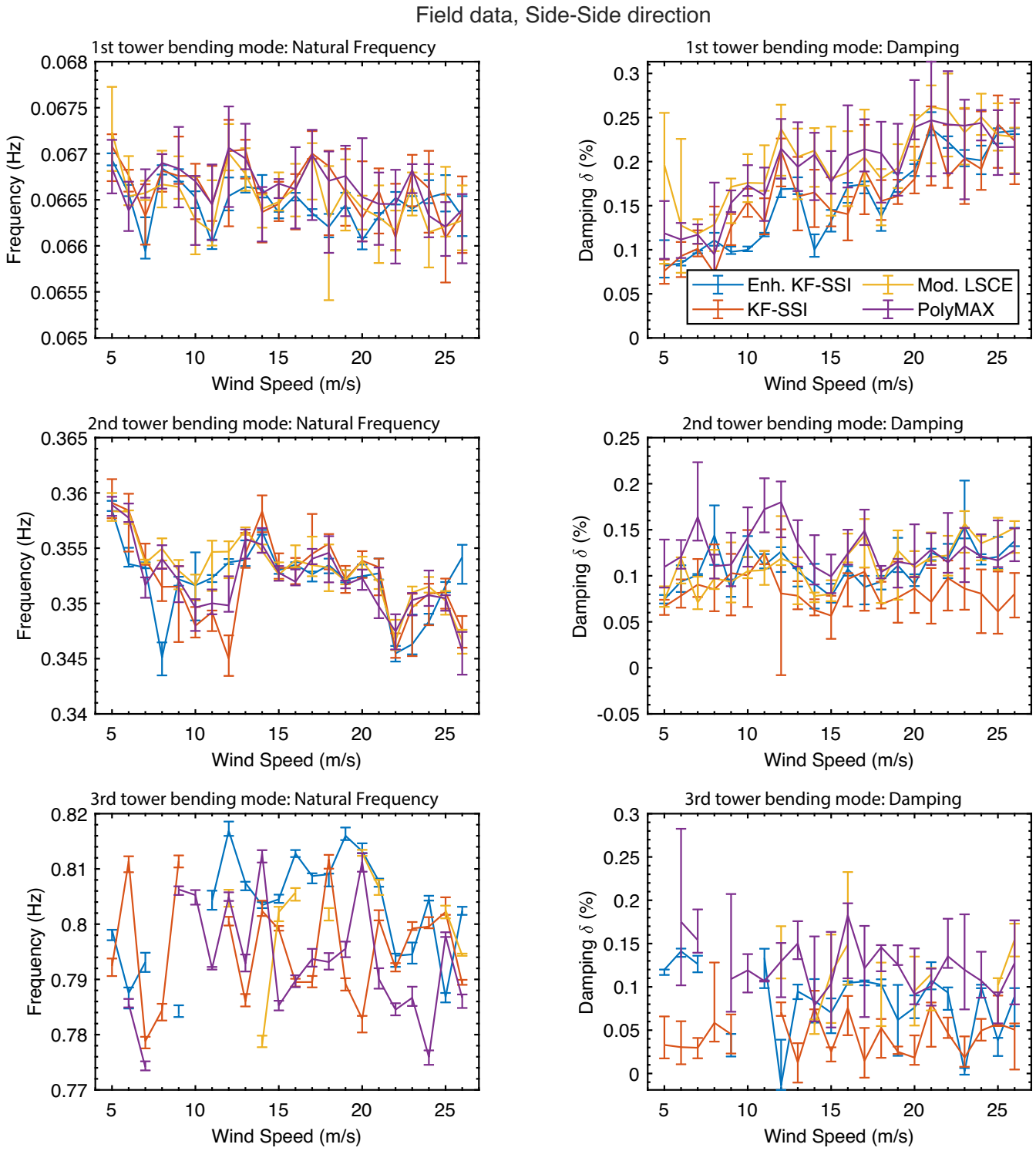


**FIGURE 13** Comparison of the estimation results of enhanced KF-SSI against PolyMAX and modified LSCE for the wind speed range. Median and variance values are given in Tables 4 to 7.

**TABLE 4** Comparison of the FA median natural frequency estimates of the enhanced KF-SSI, PolyMAX and modified LSCE algorithms at different wind speeds.

| Mode | Algorithm | 5 | 6 | 7 | 8 | 9 | 10 | 11 | 12 | 13 | 14 |
|---|---|---|---|---|---|---|---|---|---|---|---|
| First | Enhanced KF-SSI | 0.0678 | 0.0663 | 0.0663 | 0.0673 | 0.0673 | 0.0662 | 0.0675 | 0.0688 | 0.0675 | 0.0678 |
| | KF-SSI | 0.0682 | 0.0675 | 0.0689 | 0.0674 | 0.0673 | 0.0677 | 0.0675 | 0.0685 | 0.0676 | 0.0688 |
| | Modified LSCE | 0.0673 | 0.0664 | 0.0678 | 0.068 | 0.0674 | 0.0669 | 0.0672 | 0.0688 | 0.0689 | 0.0676 |
| | PolyMAX | - | - | - | 0.0688 | 0.0675 | 0.0662 | 0.0674 | 0.0687 | 0.0685 | 0.0679 |
| Second | Enhanced KF-SSI | - | - | - | 0.348 | 0.359 | 0.353 | - | 0.353 | 0.355 | 0.352 |
| | KF-SSI | - | - | - | - | - | - | 0.357 | 0.347 | 0.354 | 0.349 |
| | Modified LSCE | - | - | - | - | 0.356 | - | - | 0.352 | - | 0.356 |
| | PolyMAX | - | 0.354 | - | - | 0.347 | 0.354 | - | 0.352 | - | 0.356 |
| Third | Enhanced KF-SSI | 0.774 | - | 0.777 | 0.777 | 0.772 | 0.778 | - | 0.77 | 0.785 | 0.782 |
| | KF-SSI | - | - | - | - | - | - | - | - | - | - |
| | Modified LSCE | 0.774 | 0.779 | - | 0.774 | - | - | - | - | - | - |
| | PolyMAX | 0.772 | 0.789 | - | 0.768 | 0.793 | - | 0.77 | 0.799 | 0.771 | 0.775 |

**TABLE 4** (Continued)

| Mode | 15 | 16 | 17 | 18 | 19 | 20 | 21 | 22 | 23 | 24 | 25 | 26 |
|---|---|---|---|---|---|---|---|---|---|---|---|---|
| First | 0.0683 | 0.0691 | 0.0682 | 0.068 | 0.0692 | 0.0699 | 0.0689 | 0.0704 | 0.0687 | 0.0668 | 0.0682 | 0.0688 |
| | 0.0681 | 0.069 | 0.0674 | 0.0672 | 0.0692 | 0.0687 | 0.0688 | 0.0693 | 0.0678 | 0.0699 | 0.0701 | 0.0687 |
| | 0.0685 | 0.0692 | 0.0692 | 0.0675 | 0.0687 | 0.0695 | 0.0679 | 0.0694 | 0.069 | 0.0686 | 0.0661 | 0.0671 |
| | 0.0685 | 0.0695 | 0.0684 | - | 0.0688 | 0.0667 | 0.0677 | 0.0676 | 0.0674 | 0.0666 | 0.0665 | 0.066 |
| Second | 0.355 | - | - | 0.36 | 0.36 | 0.353 | 0.355 | 0.356 | - | - | 0.353 | 0.349 |
| | 0.352 | 0.352 | 0.352 | 0.359 | 0.346 | 0.354 | 0.354 | 0.351 | 0.348 | - | - | 0.355 |
| | 0.356 | 0.352 | 0.355 | 0.348 | - | - | - | - | 0.348 | 0.352 | - | - |
| | 0.353 | 0.355 | 0.353 | - | - | - | 0.348 | - | 0.348 | 0.353 | 0.345 | - |
| Third | 0.775 | 0.787 | 0.786 | 0.787 | 0.782 | 0.783 | 0.783 | 0.777 | 0.78 | 0.783 | 0.782 | 0.778 |
| | - | 0.794 | - | 0.782 | - | - | - | - | - | - | 0.781 | - |
| | 0.775 | - | - | 0.778 | 0.786 | - | - | 0.767 | - | 0.788 | - | 0.775 |
| | 0.767 | 0.771 | 0.782 | 0.764 | 0.8 | 0.775 | - | 0.772 | 0.774 | 0.796 | 0.779 | 0.775 |

**TABLE 5** Comparison of the FA median damping estimates of the enhanced KF-SSI, PolyMAX and modified LSCE algorithms at different wind speeds.

| Mode | Algorithm | 5 | 6 | 7 | 8 | 9 | 10 | 11 | 12 | 13 | 14 |
|---|---|---|---|---|---|---|---|---|---|---|---|
| First | Enhanced KF-SSI | 0.299 | 0.228 | 0.379 | 0.237 | 0.264 | 0.349 | 0.303 | 0.423 | 0.38 | 0.371 |
| | KF-SSI | 0.236 | 0.374 | 0.354 | 0.217 | 0.252 | 0.32 | 0.266 | 0.377 | 0.354 | 0.454 |
| | Modified LSCE | 0.213 | 0.607 | 0.372 | 0.332 | 0.325 | 0.429 | 0.326 | 0.517 | 0.453 | 0.479 |
| | PolyMAX | - | - | - | 0.297 | 0.324 | 0.379 | 0.345 | 0.445 | 0.46 | 0.519 |
| Second | Enhanced KF-SSI | - | - | - | 0.114 | 0.202 | 0.109 | - | 0.0861 | 0.126 | 0.101 |
| | KF-SSI | - | - | - | - | - | - | 0.103 | 0.0544 | 0.121 | 0.0767 |
| | Modified LSCE | - | - | - | - | 0.208 | - | - | 0.209 | - | 0.259 |
| | PolyMAX | - | 0.295 | - | - | 0.255 | 0.278 | - | 0.202 | - | 0.219 |
| Third | Enhanced KF-SSI | 0.0947 | - | 0.143 | 0.171 | 0.231 | 0.182 | - | 0.0968 | 0.193 | 0.158 |
| | KF-SSI | - | - | - | - | - | - | - | - | - | - |
| | Modified LSCE | 0.115 | 0.174 | - | 0.207 | - | - | - | - | - | - |
| | PolyMAX | 0.111 | 0.147 | - | 0.147 | 0.167 | - | 0.168 | 0.165 | 0.11 | 0.138 |

**TABLE 5** (Continued)

| Mode | 15 | 16 | 17 | 18 | 19 | 20 | 21 | 22 | 23 | 24 | 25 | 26 |
|---|---|---|---|---|---|---|---|---|---|---|---|---|
| First | 0.233 | 0.398 | 0.385 | 0.323 | 0.443 | 0.475 | 0.405 | 0.421 | 0.514 | 0.744 | 0.496 | 0.578 |
| | 0.275 | 0.378 | 0.373 | 0.276 | 0.394 | 0.405 | 0.381 | 0.363 | 0.397 | 0.422 | 0.273 | 0.382 |
| | 0.35 | 0.432 | 0.389 | 0.339 | 0.449 | 0.453 | 0.49 | 0.46 | 0.497 | 0.797 | 0.801 | 0.624 |
| | 0.391 | 0.568 | 0.652 | - | 0.645 | 0.892 | 0.78 | 0.677 | 0.859 | 0.861 | 0.918 | 0.79 |
| Second | 0.127 | - | - | 0.169 | 0.139 | 0.157 | 0.18 | 0.132 | - | - | 0.215 | 0.0867 |
| | 0.0959 | 0.0669 | 0.0591 | 0.125 | 0.0856 | 0.0607 | 0.0929 | 0.0238 | 0.0703 | - | - | 0.0848 |
| | 0.143 | 0.253 | 0.251 | 0.223 | - | - | - | - | 0.273 | 0.31 | - | - |
| | 0.25 | 0.307 | 0.235 | - | - | - | 0.284 | - | 0.271 | 0.283 | 0.341 | - |
| Third | 0.152 | 0.17 | 0.168 | 0.139 | 0.16 | 0.162 | 0.174 | 0.164 | 0.162 | 0.167 | 0.185 | 0.161 |
| | - | 0.0542 | - | 0.101 | - | - | - | - | - | - | 0.0525 | - |
| | 0.121 | - | - | 0.177 | 0.222 | - | - | 0.0918 | - | 0.297 | - | 0.128 |
| | 0.162 | 0.175 | 0.115 | 0.276 | 0.125 | 0.205 | - | 0.131 | 0.139 | 0.142 | 0.169 | 0.123 |

**TABLE 6** Comparison of the SS median natural frequency estimates of the enhanced KF-SSI, PolyMAX and modified LSCE algorithms at different wind speeds.

| Mode | Algorithm | 5 | 6 | 7 | 8 | 9 | 10 | 11 | 12 | 13 | 14 |
|---|---|---|---|---|---|---|---|---|---|---|---|
| First | Enhanced KF-SSI | 0.0669 | 0.0666 | 0.0659 | 0.0668 | 0.0667 | 0.0665 | 0.066 | 0.0665 | 0.0666 | 0.0666 |
| | KF-SSI | 0.0671 | 0.0668 | 0.0663 | 0.0668 | 0.0668 | 0.0668 | 0.0664 | 0.067 | 0.067 | 0.0664 |
| | Modified LSCE | 0.0672 | 0.0665 | 0.0666 | 0.0667 | 0.0666 | 0.0663 | 0.0662 | 0.067 | 0.0668 | 0.0664 |
| | PolyMAX | 0.0668 | 0.0664 | 0.0667 | 0.0669 | 0.0668 | 0.0667 | 0.0665 | 0.0671 | 0.0669 | 0.0666 |
| Second | Enhanced KF-SSI | 0.358 | 0.354 | 0.353 | 0.345 | 0.352 | 0.352 | 0.352 | 0.354 | 0.354 | 0.356 |
| | KF-SSI | 0.359 | 0.358 | 0.354 | 0.352 | 0.352 | 0.348 | 0.349 | 0.345 | 0.355 | 0.358 |
| | Modified LSCE | 0.358 | 0.358 | 0.354 | 0.355 | 0.353 | 0.352 | 0.355 | 0.355 | 0.357 | 0.355 |
| | PolyMAX | 0.359 | 0.358 | 0.352 | 0.354 | 0.352 | 0.35 | 0.35 | 0.35 | 0.356 | 0.355 |
| Third | Enhanced KF-SSI | 0.799 | 0.788 | 0.793 | - | 0.784 | - | 0.804 | 0.817 | 0.807 | 0.803 |
| | KF-SSI | 0.792 | 0.811 | 0.779 | 0.784 | 0.811 | - | - | 0.801 | 0.786 | 0.802 |
| | Modified LSCE | - | - | - | - | - | - | - | 0.804 | - | 0.778 |
| | PolyMAX | - | 0.786 | 0.774 | - | 0.806 | 0.805 | 0.792 | 0.805 | 0.793 | 0.813 |

**TABLE 6** (Continued)

| Mode | 15 | 16 | 17 | 18 | 19 | 20 | 21 | 22 | 23 | 24 | 25 | 26 |
|---|---|---|---|---|---|---|---|---|---|---|---|---|
| First | 0.0664 | 0.0665 | 0.0664 | 0.0662 | 0.0664 | 0.0661 | 0.0663 | 0.0665 | 0.0664 | 0.0665 | 0.0666 | 0.0663 |
| | 0.0665 | 0.0667 | 0.067 | 0.0669 | 0.0666 | 0.0663 | 0.0666 | 0.0661 | 0.0668 | 0.0666 | 0.0661 | 0.0664 |
| | 0.0665 | 0.0666 | 0.067 | 0.0663 | 0.0666 | 0.0664 | 0.0663 | 0.0662 | 0.0666 | 0.0661 | 0.0662 | 0.0663 |
| | 0.0667 | 0.0666 | 0.067 | 0.0667 | 0.0668 | 0.0665 | 0.0665 | 0.0665 | 0.0668 | 0.0663 | 0.0662 | 0.0664 |
| Second | 0.353 | 0.354 | 0.353 | 0.353 | 0.352 | 0.352 | 0.353 | 0.345 | 0.346 | 0.348 | 0.352 | 0.354 |
| | 0.353 | 0.353 | 0.354 | 0.355 | 0.352 | 0.354 | 0.353 | 0.346 | 0.35 | 0.351 | 0.351 | 0.348 |
| | 0.353 | 0.354 | 0.353 | 0.353 | 0.352 | 0.354 | 0.352 | 0.347 | 0.351 | 0.352 | 0.35 | 0.347 |
| | 0.353 | 0.352 | 0.354 | 0.355 | 0.352 | 0.352 | 0.35 | 0.347 | 0.35 | 0.351 | 0.35 | 0.346 |
| Third | 0.804 | 0.813 | 0.809 | 0.809 | 0.816 | 0.813 | 0.808 | 0.794 | 0.795 | 0.804 | 0.787 | 0.803 |
| | 0.799 | 0.79 | 0.79 | 0.812 | 0.789 | 0.783 | 0.801 | 0.792 | 0.799 | 0.8 | 0.802 | 0.789 |
| | 0.802 | 0.806 | - | 0.802 | - | 0.813 | 0.807 | - | - | - | 0.803 | 0.794 |
| | 0.785 | 0.79 | 0.794 | 0.793 | 0.796 | 0.811 | 0.79 | 0.785 | 0.787 | 0.776 | 0.798 | 0.787 |

**TABLE 7** Comparison of the SS median damping estimates of the enhanced KF-SSI, PolyMAX and modified LSCE algorithms at different wind speeds.

| Mode | Algorithm | 5 | 6 | 7 | 8 | 9 | 10 | 11 | 12 | 13 | 14 |
|---|---|---|---|---|---|---|---|---|---|---|---|
| First | Enhanced KF-SSI | 0.082 | 0.0844 | 0.0978 | 0.111 | 0.0976 | 0.0999 | 0.117 | 0.169 | 0.169 | 0.1 |
| | KF-SSI | 0.076 | 0.0928 | 0.101 | 0.0733 | 0.126 | 0.155 | 0.132 | 0.212 | 0.16 | 0.165 |
| | Modified LSCE | 0.196 | 0.127 | 0.118 | 0.129 | 0.171 | 0.176 | 0.175 | 0.237 | 0.205 | 0.213 |
| | PolyMAX | 0.119 | 0.112 | 0.117 | 0.0948 | 0.153 | 0.173 | 0.162 | 0.215 | 0.194 | 0.208 |
| Second | Enhanced KF-SSI | 0.0744 | 0.0937 | 0.101 | 0.144 | 0.0851 | 0.135 | 0.111 | 0.126 | 0.104 | 0.0914 |
| | KF-SSI | 0.0665 | 0.0784 | 0.0904 | 0.0853 | 0.103 | 0.101 | 0.125 | 0.0808 | 0.0783 | 0.0629 |
| | Modified LSCE | 0.0735 | 0.119 | 0.0711 | 0.0972 | 0.0935 | 0.105 | 0.106 | 0.119 | 0.112 | 0.078 |
| | PolyMAX | 0.11 | 0.121 | 0.164 | 0.11 | 0.112 | 0.142 | 0.172 | 0.18 | 0.135 | 0.11 |
| Third | Enhanced KF-SSI | 0.12 | 0.141 | 0.126 | - | 0.0406 | - | 0.134 | −0.0135 | 0.0948 | 0.0839 |
| | KF-SSI | 0.0329 | 0.0304 | 0.0297 | 0.0585 | 0.0454 | - | - | 0.071 | 0.0126 | 0.0756 |
| | Modified LSCE | - | - | - | - | - | - | - | 0.15 | - | 0.0558 |
| | PolyMAX | - | 0.175 | 0.154 | - | 0.109 | 0.119 | 0.107 | 0.129 | 0.15 | 0.0786 |

Abbreviations: KF-SSI, Kalman filter-based stochastic subspace identification; LSCE, least-squares complex exponential.

**TABLE 7** (Continued)

| Mode | 15 | 16 | 17 | 18 | 19 | 20 | 21 | 22 | 23 | 24 | 25 | 26 |
|---|---|---|---|---|---|---|---|---|---|---|---|---|
| First | 0.132 | 0.172 | 0.174 | 0.138 | 0.176 | 0.191 | 0.238 | 0.222 | 0.204 | 0.201 | 0.233 | 0.235 |
| | 0.145 | 0.14 | 0.191 | 0.155 | 0.161 | 0.18 | 0.245 | 0.183 | 0.203 | 0.192 | 0.242 | 0.224 |
| | 0.18 | 0.188 | 0.205 | 0.181 | 0.193 | 0.246 | 0.262 | 0.258 | 0.233 | 0.25 | 0.23 | 0.228 |
| | 0.177 | 0.207 | 0.214 | 0.21 | 0.184 | 0.239 | 0.247 | 0.242 | 0.241 | 0.244 | 0.216 | 0.217 |
| Second | 0.0775 | 0.107 | 0.0878 | 0.0937 | 0.111 | 0.0909 | 0.125 | 0.118 | 0.153 | 0.118 | 0.121 | 0.138 |
| | 0.0567 | 0.0964 | 0.104 | 0.069 | 0.0762 | 0.0864 | 0.0715 | 0.0975 | 0.0861 | 0.0806 | 0.0612 | 0.0803 |
| | 0.0801 | 0.123 | 0.144 | 0.0903 | 0.128 | 0.109 | 0.12 | 0.122 | 0.157 | 0.135 | 0.143 | 0.152 |
| | 0.0992 | 0.124 | 0.149 | 0.104 | 0.115 | 0.112 | 0.128 | 0.114 | 0.132 | 0.121 | 0.117 | 0.128 |
| Third | 0.0702 | 0.105 | 0.106 | 0.103 | 0.0619 | 0.0762 | 0.107 | 0.0934 | 0.00259 | 0.0998 | 0.0383 | 0.089 |
| | 0.025 | 0.0756 | 0.0147 | 0.0525 | 0.0251 | 0.0183 | 0.0808 | 0.0465 | 0.0184 | 0.0495 | 0.0575 | 0.0505 |
| | 0.116 | 0.149 | - | 0.0962 | - | 0.0951 | 0.115 | - | - | - | 0.102 | 0.155 |
| | 0.104 | 0.183 | 0.121 | 0.146 | 0.126 | 0.0913 | 0.101 | 0.135 | 0.12 | 0.107 | 0.0884 | 0.128 |

Abbreviations: KF-SSI, Kalman filter-based stochastic subspace identification; LSCE, least-squares complex exponential.

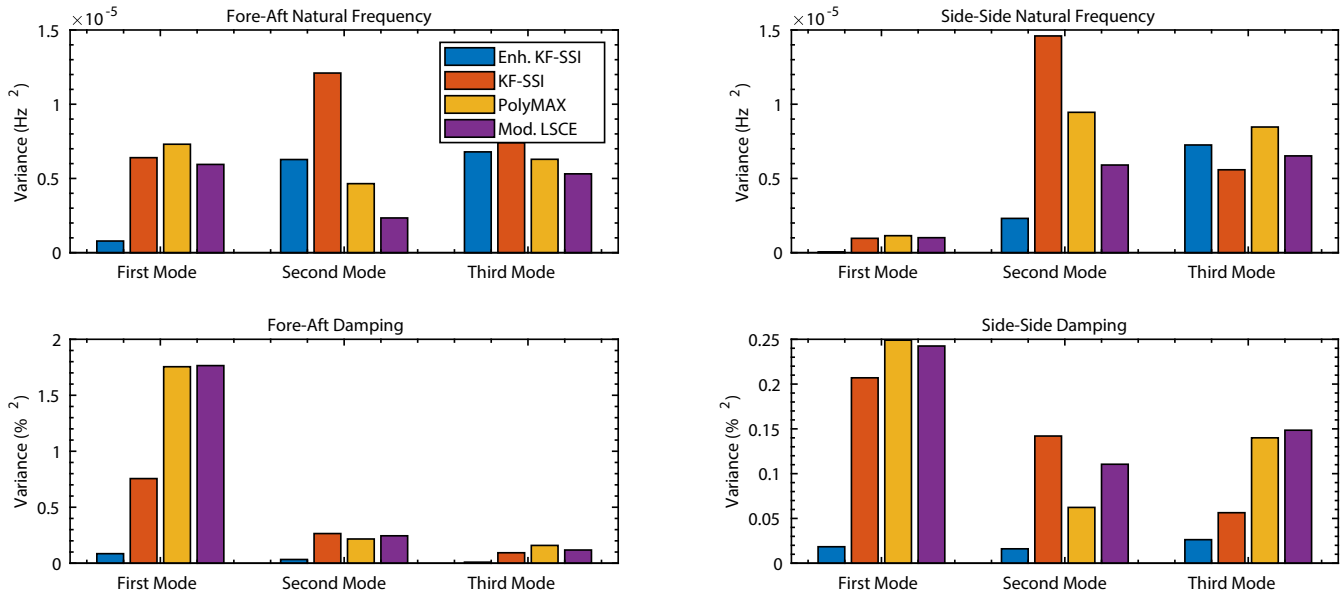


**FIGURE 14** Comparison of estimation variance between the different estimation methods. The enhanced KF-SSI has good estimation variance for the natural frequency compared to other algorithms and the estimation variance for the damping shows superiority over other algorithms.

enhanced KF-SSI algorithm accurately captures the overall trend. Also note that the enhanced KF-SSI algorithm consistently estimates higher order modes, while the other algorithms fail to do so at certain wind speeds. Moreover, although it is expected that damping increases for higher wind speeds in the first-mode FA due to aerodynamic damping, PolyMAX appears to overestimate these parameters possibly due to the lack of harmonics-mitigating steps, whereas the original KF-SSI method estimates slightly lower damping values above 18 m/s compared to the enhanced KF-SSI and modified LSCE methods.

Another comparison between the four methods, based on the variance of the estimates, is shown in Figure 14. The variance was calculated at each wind speed, and the median variance was then compared between all evaluated algorithms for each mode. The enhanced KF-SSI algorithm performs well in terms of natural frequency estimation, but its superiority becomes particularly apparent when comparing the damping values. Note that the variance for the second- and third-mode damping is significantly lower than for the first-mode damping for all identification methods, especially in the FA direction. This may be attributed to additional uncertainty introduced by aerodynamic damping at the first tower bending mode.

## 5 | CONCLUSIONS

This study demonstrated the effectiveness of the KF-SSI algorithm for identifying modal parameters from field data of an operational OWT. The KF-SSI algorithm effectively mitigates the adverse impact of harmonic disturbances, making it attractive for application to OWTs that are in operating condition.

The authors proposed an enhanced version of the KF-SSI algorithm such that multiple datasets with similar environmental conditions can be used that have been measured at different moments in time. This allows significant enhancements of the estimate precision through the use of more data. By subsequently applying the leave-one-out methodology, the median can be taken as a representative modal estimate. While enhanced KF-SSI delivers more precise estimates of modal properties, this procedure is more computationally intensive due to the data concatenation step. For the current use case of offline data processing, additional computational complexity may not be of immediate concern. However, it may pose limitations for other applications, especially for online modal analysis.

Additionally, various methods for identifying the frequencies of harmonic disturbances were evaluated as a preprocessor for the KF-SSI algorithm. The results showed that statistical methods such as Kurtosis and Entropy were not effective in identifying the frequencies of harmonics from field data of OWTs. However, it was determined that using the mean value of the rotor velocity signal as an estimate for these frequencies in the identification framework was an effective approach.

Good results were found for the damping and frequency of the first three tower bending modes using an economically attractive setup of only two accelerometer levels. With more extensive turbine instrumentation, further analyses could be conducted, and this method could also be

extended to include mode shape estimation. The results of the modal analysis using the enhanced KF-SSI algorithm were then compared to the original KF-SSI method and other, more established techniques, such as PolyMAX and modified LSCE methods. The comparison revealed that the enhanced KF-SSI method correctly captured the overall damping trend throughout the operational wind speed range, consistently, and with lower variance as compared to conventional methods.

## ACKNOWLEDGEMENTS

The authors acknowledge Siemens Gamesa Renewable Energy for their cooperation and provision of data.

## CONFLICT OF INTEREST STATEMENT

The authors declare that they have no conflict of interest.

## PEER REVIEW

The peer review history for this article is available at https://www.webofscience.com/api/gateway/wos/peer-review/10.1002/we.2849.

## DATA AVAILABILITY STATEMENT

For confidentiality reasons, the raw data cannot be shared publicly.

## ORCID

*Aemilius A. W. van Vondelen* https://orcid.org/0000-0001-9960-8339
*Sachin T. Navalkar* https://orcid.org/0000-0002-2842-9138
*Daan C. van der Hoek* https://orcid.org/0000-0002-8781-5661
*Jan-Willem van Wingerden* https://orcid.org/0000-0003-3061-7442

## REFERENCES

1. Mohanty P, Rixen DJ. Operational modal analysis in the presence of harmonic excitation. *J Sound Vib*. 2004;270(1-2):93-109.
2. Brown DL, Allemang RJ, Zimmerman R, Mergeay M. Parameter estimation techniques for modal analysis. *SAE Trans*. 1979;88:828-846.
3. Mohanty P, Rixen DJ. A modified Ibrahim time domain algorithm for operational modal analysis including harmonic excitation. *J Sound Vib*. 2004; 275(1-2):375-390.
4. Ibrahim SR, Mikulcik EC. A time domain modal vibration test technique. *Shock Vib Bull*. 1973;43(4):21-37.
5. Mohanty P, Rixen DJ. Modified SSTD method to account for harmonic excitations during operational modal analysis. *Mech Mach Theory*. 2004;39(12): 1247-1255.
6. Mohanty P, Rixen DJ. Modified ERA method for operational modal analysis in the presence of harmonic excitations. *Mech Syst Signal Process*. 2006; 20(1):114-130.
7. Dong X, Lian J, Yang M, Wang H. Operational modal identification of offshore wind turbine structure based on modified stochastic subspace identification method considering harmonic interference. *J Renew Sustain Energy*. 2014;6(3): 033128.
8. Crystal Instruments. Introduction of time synchronous averaging. https://www.crystalinstruments.com/time-synchronous-average, Crystal Instruments—Leading Innovation in Vibration Testing, Condition Monitoring, and Data Acquisition; 2016.
9. Combet F, Gelman L. An automated methodology for performing time synchronous averaging of a gearbox signal without speed sensor. *Mech Syst Signal Process*. 2007;21(6):2590-2606.
10. Randall RB, Hee J. Cepstrum analysis. *Wirel World*. 1982;88:77-80.
11. Randall RB, Peeters B, Antoni J, Manzato S. New cepstral methods of signal pre-processing for operational modal analysis. In: Proceedings of the 25th International Conference on Noise and Vibration Engineering. KU Leuven; 2012.
12. Borghesani P, Pennacchi P, Randall RB, Ricci R. Order tracking for discrete-random separation in variable speed conditions. *Mech Syst Signal Process*. 2012;30:1-22.
13. Manzato S, Devriendt C, Weijtjens W, Di Lorenzo E, Peeters B, Guillaume P. Removing the influence of rotor harmonics for improved monitoring of offshore wind turbines. *Dynamics of Civil Structures*: Springer; 2014:299-312.
14. Manzato S, White JR, LeBlanc B, Peeters B, Janssens K. Advanced identification techniques for operational wind turbine data. *Topics in Modal Analysis*, Vol. 7: Springer; 2014:195-209.
15. Randall RB, Antoni J, Smith WA. A survey of the application of the cepstrum to structural modal analysis. *Mech Syst Signal Process*. 2019;118:716-741.
16. Brincker R, Andersen P, Møller N. An indicator for separation of structural and harmonic modes in output-only modal testing. In: Proceeding of the 18th IMAC. Universidad Politécnica de Madrid; 2000.
17. Jacobsen N-J, Andersen P, Brincker R. Using EFDD as a robust technique for deterministic excitation in operational modal analysis. In: Proceedings of the 2nd International Operational Modal Analysis Conference. Aalborg Universitet; 2007:193-200.
18. Agneni A, Coppotelli G, Grappasonni C. A method for the harmonic removal in operational modal analysis of rotating blades. *Mech Syst Signal Process*. 2012;27:604-618.
19. Devriendt C, Guillaume P. The use of transmissibility measurements in output-only modal analysis. *Mech Syst Signal Process*. 2007;21(7):2689-2696.
20. Devriendt C, Guillaume P. Identification of modal parameters from transmissibility measurements. *J Sound Vib*. 2008;314(1-2):343-356.
21. Devriendt C, De Sitter G, Guillaume P. An operational modal analysis approach based on parametrically identified multivariable transmissibilities. *Mech Syst Signal Process*. 2010;24(5):1250-1259.

22. Yan W-J, Ren W-X. Operational modal parameter identification from power spectrum density transmissibility. *Comput Aided Civ Infrastruct Eng*. 2012; 27(3):202-217.
23. Yan W-J, Ren W-X. An enhanced power spectral density transmissibility (EPSDT) approach for operational modal analysis: theoretical and experimental investigation. *Eng Struct*. 2015;102:108-119.
24. Yan W-J, Zhao M-Y, Sun Q, Ren W-X. Transmissibility-based system identification for structural health monitoring: fundamentals, approaches, and applications. *Mech Syst Signal Process*. 2019;117:453-482.
25. Weijtjens W, Lataire J, Devriendt C, Guillaume P. Dealing with periodical loads and harmonics in operational modal analysis using time-varying transmissibility functions. *Mech Syst Signal Process*. 2014;49(1-2):154-164.
26. Van Overschee P, De Moor B. Subspace algorithms for the stochastic identification problem. In: Proceedings of the 30th IEEE Conference on Decision and Control, Vol. 2. IEEE; 1991:1321-1326.
27. Greś S, Döhler M, Andersen P, Mevel L. Kalman filter-based subspace identification for operational modal analysis under unmeasured periodic excitation. *Mech Syst Signal Process*. 2020;146:106996.
28. van Vondelen AAW, Navalkar ST, Iliopoulos A, van der Hoek DC, van Wingerden JW. Damping identification of offshore wind turbines using operational modal analysis: a review. *Wind Energy Sci*. 2022;7(1):161-184.
29. IEC 61400-3: 2019. Wind Energy Generation System—Part 1, Standard, International Electrotechnical Commission; 2019.
30. van der Hoek DC. Damping identification of an offshore wind turbine: a predictor-based subspace identification approach. *Master's Thesis*: Delft University of Technology; 2017.
31. Ozbek M, Rixen DJ. Operational modal analysis of a 2.5 MW wind turbine using optical measurement techniques and strain gauges. *Wind Energy*. 2013;16(3):367-381.
32. Verhaegen M. Identification of the deterministic part of MIMO state space models given in innovations form from input-output data. *Automatica*. 1994;30(1):61-74.
33. Van Overschee P, De Moor B. N4SID: subspace algorithms for the identification of combined deterministic-stochastic systems. *Automatica*. 1994; 30(1):75-93.
34. Jacobsen N-J, Andersen P, Brincker R. Eliminating the influence of harmonic components in operational modal analysis. In: Conference Proceedings: IMAC-XXIV: A Conference & Exposition on Structural Dynamics. Society for Experimental Mechanics; 2007.
35. Manzato S, Moccia D, Peeters B, Janssens K, White JR. A review of harmonic removal methods for improved operational modal analysis of wind turbines. In: Proceedings of ISMA. KU Leuven; 2012:2675-2690.
36. Döhler M, Mevel L. Fast multi-order computation of system matrices in subspace-based system identification. *Control Eng Practice*. 2012;20(9): 882-894.
37. Mastronardi N, Kressner D, Sima V, Van Dooren P, Van Huffel S. A fast algorithm for subspace state-space system identification via exploitation of the displacement structure. *J Comput Appl Math*. 2001;132(1):71-81.
38. Strang G. *Linear algebra and its applications*: Thomson, Brooks/Cole; 2006.
39. Reynders E, Houbrechts J, De Roeck G. Fully automated (operational) modal analysis. *Mech Syst Signal Process*. 2012;29:228-250.
40. Fernández Fernández P, López Aenlle M, Fernández Canteli AC, Cantieni R. Operational modal analysis of two wind turbines with foundation problems. In: 4th International Operational Modal Analysis Conference (IOMAC). Repositorio Institucional de la Universidad de Oviedo; 2011.
41. Oliveira G, Magalhães F, Cunha A, Caetano E. Continuous dynamic monitoring of an onshore wind turbine. *Eng Struct*. 2018;164:22-39.
42. Magalhães F, Cunha A, Caetano E, Brincker R. Damping estimation using free decays and ambient vibration tests. *Mech Syst Signal Process*. 2010; 24(5):1274-1290.
43. Peeters B, Van der Auweraer H. PolyMAX: a revolution in operational modal analysis. In: Proceedings of the 1st International Operational Modal Analysis Conference. Aalborg University; 2005.


**How to cite this article:** van Vondelen AAW, Iliopoulos A, Navalkar ST, van der Hoek DC, van Wingerden J-W. Modal analysis of an operational offshore wind turbine using enhanced Kalman filter-based subspace identification. *Wind Energy*. 2023;26(9):923-945. doi:10.1002/we.2849

## APPENDIX A: PROOF OF THEOREM 1

This section proves Theorem 1. First, Equations (7)–(9) are partitioned as follows:

$$Y_1 = \begin{bmatrix} Y_{11} \\ Y_{12} \end{bmatrix} = L_1 Q_1^T = \begin{bmatrix} L_{111} & 0 \\ L_{121} & L_{122} \end{bmatrix} \begin{bmatrix} Q_{11}^T \\ Q_{12}^T \end{bmatrix}, \tag{A1}$$

$$[Y_1 \;\; Y_2] = \begin{bmatrix} Y_{11} & Y_{21} \\ Y_{12} & Y_{22} \end{bmatrix} = L Q^T, \tag{A2}$$

$$[L_1 \;\; Y_2] = \begin{bmatrix} L_{111} & 0 & Y_{21} \\ L_{121} & L_{122} & Y_{22} \end{bmatrix} = L Q_\star^T. \tag{A3}$$

To demonstrate the equivalence of the $L$ matrices in Equations (A2) and (A3), which is sufficient for the KF-SSI algorithm as only the $L$ matrix is used, the property of the orthogonal $Q$ matrix, $Q^TQ = I$, can be exploited. This is done in the following by squaring Equations (A1)–(A3) and demonstrate the following equality:

$$[Y_1 \;\; Y_2][Y_1 \;\; Y_2]^T = [L_1 \;\; Y_2][L_1 \;\; Y_2]^T. \tag{A4}$$

The squares of the LQ decomposition of Equation (A1) are given as follows:

$$Y_1Y_1^T = L_1Q_1^TQ_1L_1^T = L_1L_1^T = \begin{bmatrix} L_{111} & 0 \\ L_{121} & L_{122} \end{bmatrix}\begin{bmatrix} L_{111} & 0 \\ L_{121} & L_{122} \end{bmatrix}^T, \tag{A5}$$

$$= \begin{bmatrix} L_{111}L_{111}^T & L_{111}L_{121}^T \\ L_{121}L_{111}^T & [L_{121} \;\; L_{122}][L_{121} \;\; L_{122}]^T \end{bmatrix}, \tag{A6}$$

which is the same as taking the squares as

$$Y_1Y_1^T = \begin{bmatrix} Y_{11} \\ Y_{12} \end{bmatrix}\begin{bmatrix} Y_{11} \\ Y_{12} \end{bmatrix}^T = \begin{bmatrix} Y_{11}Y_{11}^T & Y_{11}Y_{12}^T \\ Y_{12}Y_{11}^T & Y_{12}Y_{12}^T \end{bmatrix}. \tag{A7}$$

The squares of Equation (A2) yield:

$$[Y_1 \;\; Y_2][Y_1 \;\; Y_2]^T = LQ^TQL^T = LL^T = \begin{bmatrix} Y_{11} & Y_{21} \\ Y_{12} & Y_{22} \end{bmatrix}\begin{bmatrix} Y_{11} & Y_{21} \\ Y_{12} & Y_{22} \end{bmatrix}^T, \tag{A8}$$

$$= \begin{bmatrix} Y_{11}Y_{11}^T + Y_{21}Y_{21}^T & Y_{11}Y_{12}^T + Y_{21}Y_{22}^T \\ Y_{12}Y_{11}^T + Y_{22}Y_{21}^T & Y_{12}Y_{12}^T + Y_{22}Y_{22}^T \end{bmatrix} = \begin{bmatrix} Y_{11}Y_{11}^T & Y_{11}Y_{12}^T \\ Y_{12}Y_{11}^T & Y_{12}Y_{12}^T \end{bmatrix} + \begin{bmatrix} Y_{21}Y_{21}^T & Y_{12}Y_{22}^T \\ Y_{22}Y_{21}^T & Y_{22}Y_{22}^T \end{bmatrix}, \tag{A9}$$

and the squares of Equation (A3) result in

$$[L_1 \;\; Y_2][L_1 \;\; Y_2]^T = \begin{bmatrix} L_{111} & 0 & Y_{21} \\ L_{121} & L_{122} & Y_{22} \end{bmatrix}\begin{bmatrix} L_{111} & 0 & Y_{21} \\ L_{121} & L_{122} & Y_{22} \end{bmatrix}^T, \tag{A10}$$

$$= \begin{bmatrix} L_{111}L_{111}^T + Y_{21}Y_{21}^T & L_{111}L_{121}^T + Y_{21}Y_{22}^T \\ L_{121}^TL_{111}^T + Y_{22}Y_{21}^T & [L_{121} \;\; L_{122}][L_{121} \;\; L_{122}]^T + Y_{22}Y_{22}^T \end{bmatrix}, \tag{A11}$$

$$= \begin{bmatrix} L_{111}L_{111}^T & L_{111}L_{121}^T \\ L_{121}L_{111}^T & [L_{121} \;\; L_{122}][L_{121} \;\; L_{122}]^T \end{bmatrix} + \begin{bmatrix} Y_{21}Y_{21}^T & Y_{12}Y_{22}^T \\ Y_{22}Y_{21}^T & Y_{22}Y_{22}^T \end{bmatrix}. \tag{A12}$$

Observe that Equation (A6) equals Equation (A7). Equation (A7) can thus be substituted into Equation (A12) yielding Equation (A9). This proves that:

$$[Y_1 \;\; Y_2][Y_1 \;\; Y_2]^T = [L_1 \;\; Y_2][L_1 \;\; Y_2]^T, \tag{A13}$$

$$LQ^TQL^T = LQ_\star^TQ_\star L^T, \tag{A14}$$

from which it can easily be seen that both $L$ matrices are equal.